Physical-Chemical Properties of Compressible Clathrates: A Natural Pressure Shift by Extending the van der Waals and Platteeuw Model

Iuri Soter Viana Segtovich*

Escola de Química, Universidade Federal do Rio de Janeiro, Rio de Janeiro, RJ, Brazil

Fernando de Azevedo Medeiros*

Center for Energy and Resources Engineering, Department of Chemistry, Technical University of Denmark, 2800 Kongens Lyngby, Denmark

Frederico Wanderley Tavares*

Escola de Química, Universidade Federal do Rio de Janeiro, Rio de Janeiro, RJ, Brazil

Programa de Engenharia Química - PEQ/COPPE, Universidade Federal do Rio de Janeiro, Rio de Janeiro, RJ, Brazil

Abstract

We have developed a new model for compressible clathrates that extends the well-known van der Waals and Platteeuw model. The new model is derived by dispensing with the assumption of constant cages radii in the partition function level, resulting in new thermodynamically consistent expressions relating thermodynamic properties of the hydrate phase and the empty lattice isochoric reference. One set of additional parameters to the clathrate modeling framework is introduced, consisting of a scaling factor for each cage radius relative to the edge length of the unit cell. No additional guest-dependent empirical parameters are required. The model exhibits two features not previously reported in the literature: (i) a pressure shift between the clathrate being described and the empty lattice isochoric reference, and (ii) differences in the edge length of the unit cell and in the cages radii for different guest species at the same temperature and pressure, as a consequence of the sorption of guests. We also propose a test for thermodynamic consistency at high pressure, based on the multicomponent and multiphase Clapeyron equation. Using this test, we show that the proposed model solves an inconsistency issue observed in phase equilibrium calculations with some of the compressible clathrate models currently in use. We have performed parameter optimization for methane, ethane, and xenon in sI hydrates. Two sets of results are presented: 3-phase equilibrium conditions; and lattice size versus temperature or pressure for each of these substances, along with available experimental data.

Keywords:
Gas hydrate, compressibility effects, thermodynamic properties, crystallography, deformation, adsorption stress

For high-pressure conditions, additional challenges become noticeable in producing natural gas from hydrate layers on deep seafloor or flow assurance in deepwater oil fields. It has been observed that the accuracy of the standard van der Waals and Platteeuw model is not satisfactory in these scenarios. In the standard van der Waals and Platteeuw model, the specific volume of the lattice and cage radii are assumed constant. Since then, more recent experimental data show (i) variations of hydrate volume with temperature and pressure for a given guest type [1, 2, 3, 4], (ii) variation of cage radii with changing hydrate volume [5, 3], and (iii) different hydrate volume at a given temperature and pressure for different types of guests [6, 7, 8]. These phenomena are commonly labeled compressibility of clathrates and distortion of cages [9].

Volumetric information is of great importance for phase equilibrium and energy balances at high pressure. This is made evident by considering how the isothermal derivatives of the chemical potential (μ) and of the molar enthalpy $\overline{H}$ of pure substances relate to the molar volume state function $\overline{V}(T,P)$ of that substance:

$$\left(\frac{\partial \mu}{\partial P}\right)_T = \overline{V} \tag{1}$$

$$\left(\frac{\partial \overline{H}}{\partial P}\right)_T = \overline{V} - T\left(\frac{\partial \overline{V}}{\partial T}\right)_P \tag{2}$$

In fact, such information is also important for the modeling of mixtures even at low pressure, as the Langmuir coefficients are strongly dependent on the cages radii, which in turn can vary with the specific volume, which can vary with temperature and with guest species.

*Corresponding author
Email addresses: iurisegtovich@gmail.com (Iuri Soter Viana Segtovich), fermede@kemi.dtu.dk (Fernando de Azevedo Medeiros), tavares@eq.ufrj.br (Frederico Wanderley Tavares)

Volumetric information for hydrates with assumed negligible distortion has been incorporated into correlations for the specific volume of the lattice as a function of temperature and pressure [10, 11]. This information ultimately affects Poynting integrals of the empty lattice in phase equilibrium calculations.

Furthermore, the unit cell volume for a hydrate varies for different kinds of guests, according to both experiment [8] and molecular dynamics [12]. This information has usually been considered through the use of discrete guest dependent standard volume and formation properties [13, 14] or ad hoc non-ideality corrections to the expressions from the standard van der Waals and Platteeuw model to compensate for deviations from the model premises [5].

According to the Cell theory of Lennard-Jones and Devonshire [15], the Langmuir coefficients depend on the cage radii according to a free volume integral. Considering that changes in the specific volume of the hydrate might affect these dimensions, the inclusion of this dependency empirically propagates variations in lattice volume into the calculation of Langmuir coefficients and strongly affecting the calculation of occupancy [5, 16]. By using parameters regressed from hydrate phase equilibrium data, this method allowed improved data representation at high pressure. However, this was achieved at the expense of having additional parameters for each guest component and each type of cage of each structure.

We have analyzed this approach of modifications of the vdW&P model and noticed that it results in a thermodynamic inconsistency in phase equilibrium calculations. The inconsistency is made evident in this work by using a test for thermodynamic consistency based on the Clapeyron equation that we proposed. This inconsistency happens because these modifications invalidate the premise of constant cage radii, a premise on which all expressions for derived properties in the original van der Waals and Platteeuw model are based, and current modifications use those same expressions.

Here, we propose an improved model for hydrates by considering the compressibility of lattices and consecutive distortion of cages. We revise the fundamentals of statistical thermodynamics needed to derive a thermodynamic model for a clathrate solution and the assumptions made in the original van der Waals and Platteeuw model at the partition function level. Then we carry out the mathematical procedure for obtaining expressions for derived properties considering this dependency.

The development of this model was started by Segtovich [17] and was named the Pressure Shift model; it has been noted in the review by Medeiros et al. [9]. Here, we present the complete equations for the model, an iterative algorithm required for the calculation of pressure of the lattice, and quantitative results for phase equilibrium and volumetric properties after parameter estimation for methane, ethane and xenon hydrates in s^I structure. As far as we know from current literature, no other thermodynamic model in this scale can explain or predict the observations regarding lattice volume changes for hydrates of different guests relative to the empty lattice.

1. The Pressure Shift model

1.1. Motivation for a new compressible model

From the aforementioned experimental observations, we see that the molar volume of the lattice ($\overline{V}^{EL}$) depends on the composition of guest components in the hydrate associated with occupancy Θ_{ij}. We can also recognize a relation between the cages radii and the molar volume of the lattice. Consequently, this affects the Langmuir coefficients C_{ij}, which dictates the occupancy. These relations show interdependence between the variables that describe the hydrate. Finally, the occupancy directly affects the chemical potential of water in the hydrate, influencing phase equilibrium conditions even at low pressure as represented in Eq. (3).

$$\underbrace{\overline{V}^{EL}(\underline{\Theta}) \rightarrow \underline{R}\left(\overline{V}^{EL}\right) \rightarrow \underline{C}(\underline{R}) \rightarrow \underline{\Theta}(\underline{C})}_{\text{interdependent}} \rightarrow \Delta\mu_w^{H-EL} \quad (3)$$

where the molar volume of the lattice ($\overline{V}^{EL}$) corresponds to the ratio between the hydrate volume (V^H) and the number of water molecules N_w in the lattice (Eq. 4):

$$\overline{V}^{EL} = \frac{V^H}{N_w} \quad (4)$$

The pressure shift model proposed here is a rigorous extension of the vdW&P model to contemplate compressible hydrate with cage distortion. By having varying cages radii with lattice volume, and varying lattice volume with temperature and pressure, we calculate a pressure shift between the hydrate and the empty lattice isochoric reference at the same temperature. That pressure shift is responsible for varying actual hydrate volume for standard temperature and pressure for different guest types. Our calculations of pressure shift and volume can be understood in the steps presented in Fig. 1).

In Fig. 1, the hydrate is represented by a blue square for the lattice with gray circles for the cages. From one sole standard empty lattice having volume V_0 at pressure P_0 (d), consider first the enclathration of guest molecules of species 1 (green ellipsis), which has a big molecular dimension (*a large guest*) such that they will fit tightly in the larger cages (d $\rightarrow$ e). In that process, the hydrate has volume equal to that of the isochoric reference lattice (V_0), by definition in the vdW&P model. However, we can calculate a pressure difference ΔP, which for a large guest turns out to be positive ($\Delta P > 0 \therefore P > P_0$). Now, in order to calculate the volume that this hydrate would show at pressure P_0 (b) we would need to consider

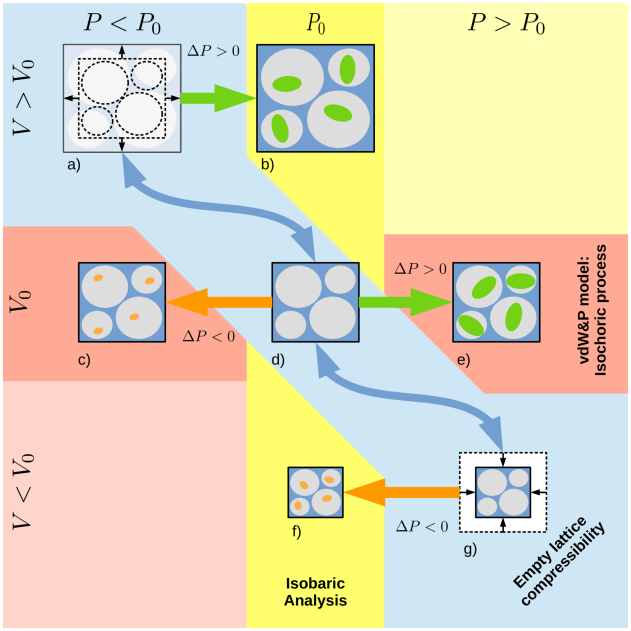

Figure 1: Schematic representation of how the pressure shift is responsible for volume differences for hydrates of different guests at the same pressure: (→) blue arrows show the relation between Volume and Pressure due to the intrinsic compressibility of the empty lattice ; (→, →) green and orange arrows show the pressure shift that occurs with adsorption at constant volume from the isochoric empty lattice reference; (•) green ellipsis are guest species with relatively large molecular size, causing lattice expansion, (•) orange ellipsis are guest species with relatively small molecular size, causing lattice contraction.

the process of enclathration from an isochoric empty lattice reference at $P^{\mathrm{EL}} < P_0$ (a), so that $P^{\mathrm{EL}} + \Delta P^{(+)} = P_0$ (a → b). Because of the intrinsic compressibility of the empty lattice (blue left-right arrows), the volume of the empty lattice at pressure slightly lower than P_0 should be slightly larger than V_0 (d → a). Based on this pressure shift reasoning, we can conclude that the volume of a hydrate of a large guest at P_0 (b) is larger than the volume of the reference lattice at that same P_0 (d), $V > V_0$. Analogously, for a guest component of species 2, which has a lower molecular dimension such that it fits loosely in the cages (*a small guest*), calculations show that the pressure difference is negative $\Delta P < 0 \therefore P < P_0$ (d → c). Then, in order to calculate the volume that this hydrate would show at pressure P_0 (f) we would need to consider the process of enclathration from an isochoric empty lattice reference at $P^{\mathrm{EL}} > P_0$ (g), so that $P^{\mathrm{EL}} + \Delta P^{(-)} = P_0$ (g → f). We conclude that the hydrate volume at P_0 (f) is smaller than that of the reference lattice at that same P_0 (d), $V < V_0$. These two cases show how the pressure shift contribution can result in the volume of a hydrate of large guests being greater than that of small guests, due to expansion and contraction of the lattice. Note that there are competing effects between tightness and looseness of each species in each cage that add up to the overall pressure shift ($\Delta P = P^{\mathrm{H}} - P^{\mathrm{EL}}$). Also, the pressure shift contribution at a given P depends on the unknown occupancy Θ_{ij} and reference lattice volume $\overline{V}^{\mathrm{EL}}(P^{\mathrm{EL}})$, so the actual implementation requires an iterative scheme detailed in Section 1.9.

It is worth mentioning that the deformation of porous matrix by adsorption is a topic that has long driven the attention of the scientific community. Vandamme [18] identifies a surge in those studies in recent years due to the popularity of materials that exhibit deformations upon adsorption, such as metal-organic frameworks. Works trying to establish a link between thermodynamic properties and adsorption stress have also focused on applications with biopolymers [19] and gas adsorption on coal [20, 21], for example. One of the most pertinent studies to the one we develop here is the one by Ravikovitch and Neimark [22]. Using density functional theory (DFT), the authors showed natural elastic stress and volumetric strain from a thermodynamic potential (Ω) whose independent variables were T, V and μ of the adsorbates. The stress produced by adsorption is proportional to the marginal change of Ω with the radius of the pores. Therefore, the compressible clathrate model presented here belongs to some extent to this class of models, whose goal is to quantify the mechanical changes (pressure and volume interplay) in a given matrix due to adsorption.

1.2. *The partition function*

The original van der Waals and Platteeuw [23] model is constructed using a partition function that describes the clathrate phase as a solid mixture, which is a function of the number of water molecules (N_{w}) and the number of the so-called guest components molecules (N_i^{g}) of a few types (n^{g}), temperature T and volume V^{H} of the phase. The final formulation of the model is obtained from the following assumptions:

1. There is an a priori description of a lattice of water molecules at the same temperature T, having an equal volume ($V^{\mathrm{EL}} = V^{\mathrm{H}}$) and an equal number of water molecules (N_{w}), containing N_j^{c} identical cages of a few types (n^{c});

2. A guest molecule is always located inside some cage, and one individual cage can never hold more than one guest molecules simultaneously; and

3. Interactions between guest molecules are negligible.

With these premises, they devised a partition function in the canonical ensemble and transformed that into a semi-grand canonical partition function for convenience in dealing with phase equilibrium calculations [23, 9].

The semi-grand canonical partition function (Ξ) represents an ensemble contemplating varying number (N_{ij}) of particles of each guest component (i) in each cage type (j) for a given chemical potential for each guest component (μ_{ij}), a given number of water molecules (N_{w}) a

given temperature (T) and a given phase volume (V^{H}). It is expressed as

$$\ln \Xi = \ln Q^{\mathrm{EL}} + \sum_j \left(\nu_j N_{\mathrm{w}} \ln \left(1 + \sum_i \left(q_{ij} \lambda_{ij} \right) \right) \right) \tag{5}$$

where ($\underline{\nu}$) are proportionality factors that relate the number of cages of each type to the number of water molecules in the hydrate phase and depends solely on the a priori described lattice geometry, and (λ_{ij}) are the so-called absolute activity, conjugated to N_{ij}, defined for each guest component in each cage type in the hydrate phase from its chemical potential (μ_{ij}), temperature (T) and Boltzmann constant k_{B} by

$$\mu_{ij} = k_{\mathrm{B}} T \ln \left(\lambda_{ij} \right) \tag{6}$$

Here, Q^{EL} is the canonical partition function describing the pure water empty lattice by its temperature, volume, and the number of water molecules (Section 1.3), and q_{ij} is the single-molecule canonical partition function under the mean-field cage potential (Section 1.4).

The semi-grand-canonical partition function is associated with the thermodynamic potential we denote by Ψ, resulting from the Legendre transform of the Helmholtz energy (A) switching each N_{ij} for the corresponding μ_{ij} as done in the transformation of the partition function from the canonical to semi-grand-canonical ensemble under its formalism [9]. Therefore, these thermodynamic potentials are related to each other and with the partition function by

$$\Psi = A - \sum_i \sum_j \left(N_{ij} \mu_{ij} \right) = -k_{\mathrm{B}} T \ln \Xi \tag{7}$$

1.3. The empty lattice reference

The canonical partition function of the empty lattice is related to the Helmholtz energy by

$$A^{\mathrm{EL}} = -k_{\mathrm{B}} T \ln Q^{\mathrm{EL}} \tag{8}$$

where its differentials, from classical thermodynamics are

$$\mathrm{d}A^{\mathrm{EL}} = -S\mathrm{d}T - P\mathrm{d}V^{\mathrm{EL}} + \mu_{\mathrm{w}}^{\mathrm{EL}} \mathrm{d}N_{\mathrm{w}} \tag{9}$$

$$\mathrm{d}\left(\frac{A^{\mathrm{EL}}}{k_{\mathrm{B}} T} \right) = -\frac{U^{\mathrm{EL}}}{k_{\mathrm{B}} T^2} \mathrm{d}T - \frac{P^{\mathrm{EL}}}{k_{\mathrm{B}} T} \mathrm{d}V^{\mathrm{EL}} + \frac{\mu_{\mathrm{w}}^{\mathrm{EL}}}{k_{\mathrm{B}} T} \mathrm{d}N_{\mathrm{w}} \tag{10}$$

From these, derived properties as chemical potential, internal energy and pressure can be calculated from the partition function by

$$\mu_{\mathrm{w}}^{\mathrm{EL}} = k_{\mathrm{B}} T \left(\frac{\partial A^{\mathrm{EL}} / k_{\mathrm{B}} T}{\partial N_{\mathrm{w}}} \right)_{T, V^{\mathrm{EL}}} \tag{11}$$

$$U^{\mathrm{EL}} = -k_{\mathrm{B}} T^2 \left(\frac{\partial A^{\mathrm{EL}} / k_{\mathrm{B}} T}{\partial T} \right)_{V^{\mathrm{EL}}, N_{\mathrm{w}}} \tag{12}$$

$$P^{\mathrm{EL}} = -k_{\mathrm{B}} T \left(\frac{\partial A^{\mathrm{EL}} / k_{\mathrm{B}} T}{\partial V^{\mathrm{EL}}} \right)_{T, N_{\mathrm{w}}} \tag{13}$$

These expressions are crucial for the symbolic derivations conducted here, as the canonical partition function for the empty lattice has precisely T, V^{EL}, and N_{w} as independent variables.

1.4. Cell theory and the Langmuir coefficients

In order to describe the partition function for a single enclathrated molecule under the mean field cage potential (q_{ij}), additional considerations are necessary [23].

4. Internal degrees of freedom of that guest molecule are equivalent to those of that molecule in the ideal gas state,

5. Translation inside the cage is subject to a mean-field water-guest potential based on the approximation of Lennard-Jones and Devonshire.

From those assumptions, q_{ij} is given by a product of a term for internal degrees of freedom (Φ_i) and an integral for the free volume:

$$q_{ij} = \Phi_i \int_0^{R_j} \left[\exp \left(\frac{-w_{ij}}{k_{\mathrm{B}} T} \right) 4\pi r^2 \right] \mathrm{d}r \tag{14}$$

The factor Φ_i represents the configurational integral for internal degrees of freedom (as rotation and vibration) and particle momentum (thermal de Broglie wavelength), which is component specific and solely a function of temperature. The configurational integral for the free volume is evaluated for the mean-field cage potential w_{ij} along with radial coordinate r in the domain of a cell with radius R_j.

In addition, it is helpful to relate absolute activity ($\underline{\lambda}$) to fugacity ($\hat{f}$) using the ideal gas partition function as a reference [24]:

$$\hat{f}_{ij} = \lambda_{ij} k_{\mathrm{B}} T \Phi_i \tag{15}$$

This expression carries that same factor (Φ_i), in accordance to assumption 4.

Using these, Langmuir coefficients (C_{ij}) are defined from the following relation:

$$q_{ij} \lambda_{ij} = C_{ij} \hat{f}_{ij} \tag{16}$$

so that derived properties expressions can be rewritten in terms of finite C_{ij} and $\hat{f}_{ij}$ for practical calculations.

We can express Langmuir coefficients from the free volume integral as

$$C_{ij} = \frac{\int_0^{R_j} \left[\exp \left(-w_{ij} / k_{\mathrm{B}} T \right) 4\pi r^2 \right] \mathrm{d}r}{k_{\mathrm{B}} T} \tag{17}$$

where the factor (Φ_i) from Eq. (14) and Eq. (15) cancels out, and we can express q_{ij} from C_{ij}, for convenient symbolic calculations as in

$$q_{ij} = k_B T \Phi_i C_{ij} \tag{18}$$

We have used the cage potential w_{ij} derived from the Kihara pair interaction potential. This cage potential forbids the particle from being closer to the cage boundary by less than a hard-core interaction parameter a_i; thus, the implementation of Eq. 17 has this information built into its upper limit of integration as $(R_j - a_i)$ [25]. The resulting expression for w_{ij} is given by [23, 26, 27, 9]; see Appendix A.

The Langmuir coefficients depend on cages radii, as calculated from the cell theory for hydrates; this is illustrated in Fig. 2.

The cage potential w_{ij} depends on the radial coordinate of a guest inside an assumed spherical cage (r), in addition to the structural parameters such as the coordination number of water molecules per cage (Z_j) and the cage radius (R_j), as well as the effective interaction parameters between guest and host molecules (a_i, σ_i, ϵ_i). Langmuir coefficients, coming from the configurational integral over the radial coordinate, are dependent on temperature and those structural and interaction parameters. The Langmuir coefficient at constant temperature shows a maximum with respect to cage radius (Fig. 2a). For a cage whose radius is large relative to the molecule size, the molecule fits loosely into the cage; consequently, attractive interaction predominates. Thus, the cage potential energy decreases for a slightly smaller cage radius, and Langmuir coefficients increase. This may happen up to a point where the cage is small enough so that the molecule fits tightly. Then, for an even smaller cage radius, repulsive interaction predominates, cage potential energy increases, and Langmuir coefficients decrease.

Plotting Langmuir coefficients as a function of temperature for small perturbations of the cage radius (Figures 2b) shows that decreasing the radius for a cage in which the guest molecule fits tightly will make it too tight and increase the predominance of repulsive force, and the curve of Langmuir coefficient versus temperature is shifted down, (blue curves). On the other hand, decreasing the radius for a cage in which the guest component molecule fits loosely will make it less loose and increase the predominance of attractive force, and the curve of Langmuir coefficient versus temperature is shifted up (orange curves).

Note that, by considering varying cage radius under the approximation of Lennard-Jones and Devonshire, we intend to represent isotropic cage deformations, i.e., keeping the radial symmetry.

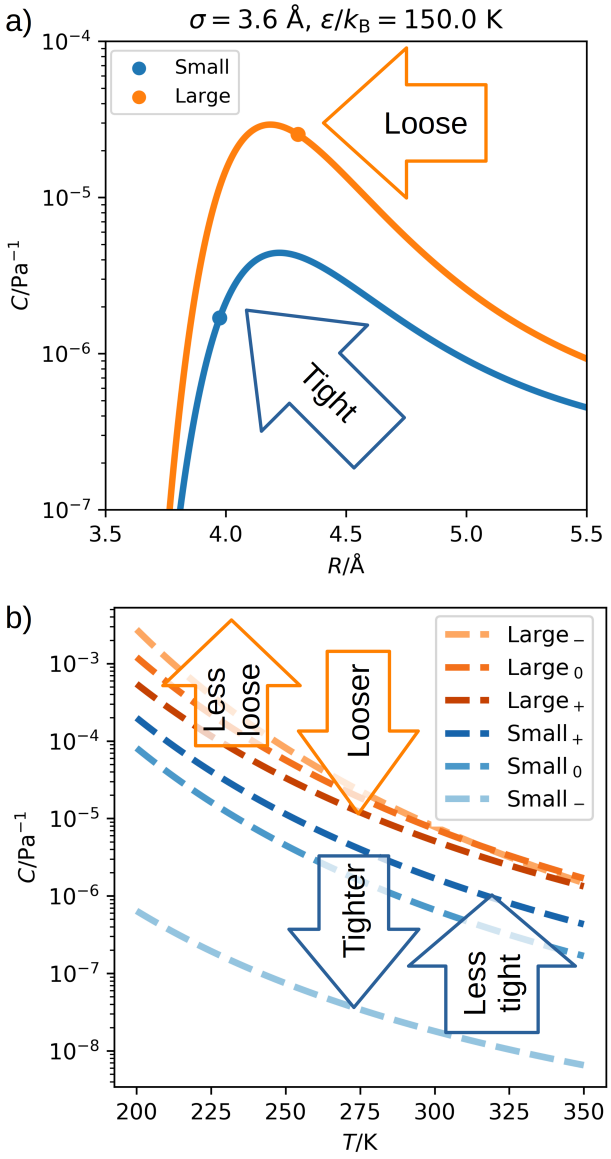

Figure 2: Langmuir coefficients depend on cages radii, as calculated from the cell theory for hydrates. (a) (•, •) bullets show the Langmuir coefficients for a hypothetical molecule in the small (blue) and large (orange) cages of a s^I hydrate given for a lattice with specified molar volume, where a given guest is tightly or loosely fit, respectively; (—, —) lines show the Langmuir coefficients given as a function of that cage radius at fixed molecular radius σ; (b) Langmuir coefficients for a hypothetical molecule versus T in the small and large cages of a s^I hydrate given for a lattice with specified molar volume (Small$_0$, Large$_0$), and given for small positive (+) and negative (-) perturbations of the cage radius.

1.5. Geometry relation between cages radii and lattice molar volume

We can relate the cages radii to the lattice molar volume, showing that R_j depends on both the extensive volume of the lattice and on the number of water molecules as independent variables in the semi-grand-canonical partition function. This will be crucial for the reasoning and mathematical derivations that follow.

Consider a cubic unit cell with N_0 molecules and edge length a_0, therefore with volume a_0^3. Fig. 3 shows that a is a function of the lattice molar volume and, therefore, in the calculations to be performed, it is a function of both extensive lattice volume at constant mole number and function of mole number at constant extensive lattice volume.

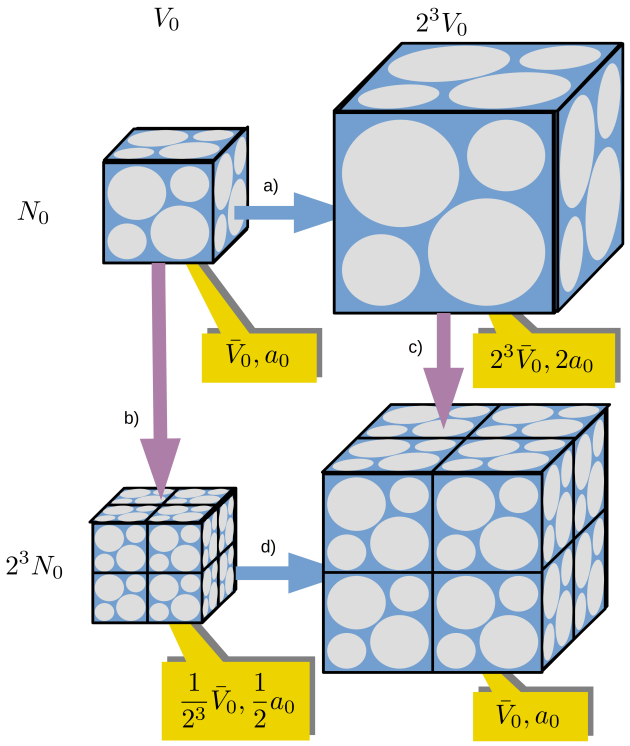

Figure 3: Geometric relation between the edge length of the unit cell with number of molecules, extensive volume and molar volume of the lattice: (→) blue arrows show increase in volume at constant number of molecules, resulting in unit cell expansion, (→) purple arrows show increase of number of molecules at constant volume, resulting in unit cell contraction.

Increasing the extensive volume from V_0 to 2^3V_0 while holding constant N_w at N_0, which is done by expanding existing unit cells (paths a or d), results in a larger molar lattice volume and larger edge length. Alternatively increasing the number of water molecules N_w from N_0 to 2^3N_0 holding constant the extensive lattice volume (paths b or c), which is obtained by increasing the number of unit cells scaled down to fit in the same volume, results in a smaller molar lattice volume and smaller edge length. When changing both extensive and number of molecules simultaneously, one keeps constant the molar lattice volume and thus edge length (paths a+c or b+d).

Furthermore, there is evidence of variation of the radius of each cage type with the unit cell lattice parameters from molecular simulations [5] and from experimental data [3]. In this spirit, we shall proceed to relate the lattice molar volume with the edge length of the unit cell and with cages radii according to the following geometrical relations:

1. The unit cell is a basic unit from which the macroscopic phase is described by means of simple replication. The unit cell has constant number of molecules (N_w^{uc}) and its specific volume (V_{uc}/N_w^{uc}) is equal to the macroscopic lattice molar volume $\overline{V}^{EL}$.

$$\overline{V}^{EL} = \frac{V^H}{N_w} = \frac{V^{uc}}{N_w^{uc}} \tag{19}$$

$$d\overline{V}^{EL} = d\left(\frac{V^H}{N_w}\right) = \frac{1}{N_w^{uc}} dV^{uc} \tag{20}$$

2. The unit cell is cubic, with variable edge length a_{uc}

$$V_{uc} = {a_{uc}}^3 \tag{21}$$

$$dV^{uc} = 3{a_{uc}}^2 da_{uc} \tag{22}$$

3. The shells radii for the water molecules coordinating a cage are empirically correlated to the edge length. Therefore we have considered, for the mean radii in the Lennard-Jones-Devonshire approximation, the following expression with a scaling parameter k_{Rj}:

$$R_j = R_{j,0}\left(\frac{a_{uc}}{a_{uc,0}}\right)^{\frac{k_{Rj}}{k}} \tag{23}$$

$$\frac{\partial R_j}{\partial a_{uc}} = \frac{R_{j,0}k_{Rj}}{a_{uc,0}k}\left(\frac{a_{uc}}{a_{uc,0}}\right)^{\frac{k_{Rj}}{k}-1} \tag{24}$$

where k_{Rj} is a scaling factor for each cage radius with respect to the edge length of the unit cell.

In the trivial case, where $k_{Rj} = 0$, the radii are constant and the derivative is null. In the simplest case, apart from that, where $k_{Rj} = k$, for each cage type j, cages radii are proportional to the edge length, and the derivative is the $R_{j,0}/a_{uc,0}$ constant factor. These parameters (k_{Rj}) are included in the optimization scheme performed here to better represent phase equilibrium and volumetric data of the selected components (Section 3.1).

As the Langmuir coefficients depend on the cage radius, this variable dependence scheme finally leads to the following effective relation of Langmuir coefficients and lattice molar volume, which will be useful in subsequent symbolic calculations:

$$\frac{\partial C_{ij}}{\partial \overline{V}^{EL}} = \frac{\partial C_{ij}}{\partial R_j}\frac{\partial R_j}{\partial a_{uc}}\frac{\partial a_{uc}}{\partial V_{uc}}\frac{\partial V_{uc}}{\partial \overline{V}^{EL}} \tag{25}$$

Since $\partial R_j/\partial a_{uc}$, $\partial a_{uc}/\partial V_{uc}$, $\partial V_{uc}/\partial \overline{V}^{EL}$ are all positive, it is worthwhile to notice that the sign of $\partial C_{ij}/\partial \overline{V}^{EL}$ is determined by the slope of C_{ij} with respect to R_j (Fig. 2a).

Note also that the relation presented in Fig. 3 and Eqs. 19 to 25 support attaining to any empirical relation between R_j and a_{uc} suggested from measurements or molecular simulations by means of changing Eq. 23 and 24 accordingly. For detailed steps regarding the determination of each of these terms in this work, see Appendix A.

1.6. Volumetric properties for the empty lattice

Although the literature has shown possible theoretical models for an empty lattice volume [28], we have chosen to work with a simple correlation. We use an empirical expression to relate pressure and temperature to the volume of the empty lattice, as a pure water crystalline phase, based on the assumptions of constant isothermal compressibility and a polynomial isobaric edge length behavior, in a *per mol* basis:

$$\frac{\overline{V}^{EL}}{m^3 mol^{-1}} = \left(\frac{a_{uc,0}}{\text{Å}} + \alpha_1 \left(\frac{T}{K} - \frac{T_{uc,0}}{K} \right) + \alpha_2 \left(\frac{T}{K} - \frac{T_{uc,0}}{K} \right)^2 \right)^3 \times \frac{10^{-30} N_A}{N_{w,uc}} \exp\left(-\frac{k}{Pa^{-1}} \left(\frac{P}{Pa} - \frac{P_{uc,0}}{Pa} \right) \right) \quad (26)$$

where N_A is the Avogadro number, $a_{uc,0}$ is the edge length of the unit cell at $P = P_{uc,0}$ and $T = T_{uc,0}$.

This expression allows one to relate the pressure and volume of the empty lattice. However, experimental data is only available for actual clathrates. Recalling that the hydrate modeled with the vdW&P model has volume V^H equal to the empty lattice reference V^{EL} but not the same pressure, the parameters in the correlation for V^{EL} were regressed from crystallography measurements for the hydrate volume V^H by considering the pressure shift calculation. We also used results from theoretical Lattice Dynamics (LD) calculations for volumetric properties of the empty lattice performed by Belosludov and collaborators [28] in the regression; we achieved a compromise between representing LD data for the empty lattice and hydrate experimental data for different guests.

1.7. Thermodynamic properties for compressible hydrates

We have obtained thermodynamic properties for compressible hydrates via symbolic calculations taking the dependence of each q_{ij} with V^H/N_w into consideration. The expressions for N_{ij} and Θ_{ij}, are the same as before, however the expression for pressure and chemical potential, which are based on partial derivatives with respect to V^H and N_w, respectively, will both get an extra contribution when considering each R_j dependent on V^H/N_w [9].

The hydrate thermodynamic potential is related to the Helmholtz energy by Eq. (7), and therefore it can be shown that its differential form, from classical thermodynamics, is

$$d\left(\frac{\Psi}{k_B T}\right) = -\frac{U}{k_B T^2} dT - \frac{P}{k_B T} dV^H + \frac{\mu_w}{k_B T} dN_w - \sum_{ij} \left[N_{ij} d\ln\left(\lambda_{ij}\right) \right] \quad (27)$$

1.7.1. Occupancy

Inspecting Eq. (27), one can relate the number of guest molecules with the partition function by

$$N_{ij} = -\left(\frac{\partial \Psi / k_B T}{\partial \ln \lambda_{ij}} \right)_{T, V^H, N_w, \lambda_{\neq ij}} \quad (28)$$

from which it is convenient to define the occupancy fraction (Θ_{ij}) of type j cages by molecules of type i as

$$\Theta_{ij} = \frac{N_{ij}}{\nu_j N_w} \quad (29)$$

The occupancy fraction (Θ_{ij}) of type j cages by molecules of type i is, as a result of that derivative of the clathrate potential, given by:

$$\Theta_{ij} = \frac{q_{ij}\lambda_{ij}}{\sum_k \left[q_{kj}\lambda_{kj} \right] + 1} = \frac{C_{ij}\hat{f}_{ij}}{\sum_k \left[C_{kj}\hat{f}_{kj} \right] + 1} \quad (30)$$

From this, the partition function can be rewritten, for use in subsequent derivations, as

$$-\frac{\Psi}{k_B T} = \ln \Xi = \ln Q^{EL} - \sum_j \left(\nu_j N_w \ln\left(1 - \sum_i \left(\Theta_{ij} \right) \right) \right) \quad (31)$$

using the algebraic identity that

$$\sum_i \left(q_{ij}\lambda_{ij} + 1 \right) = 1 / \left(1 - \sum_i \left(\Theta_{ij} \right) \right) \quad (32)$$

1.7.2. Hydrate pressure

We can calculate the hydrate pressure in the thermodynamic state described by T, V^H, N_w and $\underline{\lambda}$. Inspecting Eq. (27), pressure is related to the partition function according to

$$P^H = -k_B T \left(\frac{\partial \Psi / k_B T}{\partial V^H} \right)_{T, N_w, \underline{\lambda}} \quad (33)$$

Applying this operation and using Eqs. 31 and 27 we obtain

$$P^H = -\frac{\partial A^{EL}}{\partial V^{EL}} - k_B T \sum_j \left[\nu_j N_w \frac{\partial \ln\left(1 - \sum_i \left[\Theta_{ij}\right]\right)}{\partial V^H} \right] \quad (34)$$

where the empty lattice term corresponds to the pure water empty lattice phase pressure in the condition of $V^{EL} = V^{H}$, N_w and T (Eq. 13). We then define the difference in pressure between hydrate having $\underline{\lambda}$ activity of guests and the empty lattice at that condition by ΔP^{H-EL}, which we refer to as the pressure shift.

Applying the product and chain rules for derivatives of the partition function with respect to extensive volume at constant water mole number, and recalling Eq. (4) and Fig. 3 we obtain the final expression for the pressure shift, with all properties in *per mol* basis, as

$$\Delta P^{H-EL} = P^{H} - P^{EL} = RT\left(\sum_j\left[\nu_j\sum_i\left[\frac{\Theta_{ij}}{C_{ij}}\left(\frac{\partial C_{ij}}{\partial \overline{V}^{EL}}\right)_T\right]\right]\right) \quad (35)$$

The applicable form of this expression depends on either a partition function for the enclathrated molecules (Eq. 14) or an empirical expression for Langmuir coefficients with explicit dependence on the lattice molar volume fitted to either rigorous model results [26] or to phase equilibrium data.

One can draw interesting conclusions by comparing Equation 35 to Equation 25. Since all terms multiplying $\partial C_{ij}/\partial \overline{V}^{EL}$ in Equation 35 are positive, the sign of the pressure shift will result from a combination of the signs of the slopes of C_{ij} with respect to R_j for all cage types. From Fig. 2b, one can see that there are equal values of C_{ij} for different values of R_j. Thus, the pressure shift can help distinguish between the values of cage radius that yield the same C_{ij} and, consequently, the same Θ_{ij}.

Note that in the case of considering that the Langmuir coefficient itself does not vary with the lattice molar volume, as in the case where the R_j was not related to V^{H}/N_w through our geometry considerations, the ΔP^{H-EL} would vanish naturally: the pressure in the empty lattice would be equal to the actual hydrate pressure. This is a common simplification in current literature, but would be the case of a hydrate capable of interstitial compressibility while keeping cages size constant, which is at best a rough approximation for small compressibility. This case is referred to in the results and discussion section as the *Interstitial* model.

In the general case, one can say that the lattice does "see" the guest component molecules, so much that (a) the pressure of the phase significantly increases or decreases with the adsorption extent at constant volume or alternatively (b) the volume does vary in function of occupancy at a constant pressure analysis.

For phase equilibrium calculations, it should be clear that the hydrate pressure is equal to each of the other bulk phases pressure, as it is the thermodynamic property conjugated to the volume of the actual hydrate phase, while the lattice pressure P^{EL} gives the hydrate phase volume according to the intrinsic volumetric relation of the empty lattice.

For details on the determination of $\left(\frac{\partial \ln(C_{ij})}{\partial \overline{V}^{EL}}\right)_T$, see Appendix A.

1.7.3. *Chemical potential of the host component*

The chemical potential of water, by inspection of 27 is related to the partition function according to

$$\mu_w^{H} = k_B T\left(\frac{\partial \Psi/k_B T}{\partial N_w}\right)_{T,V^{H},\underline{\lambda}} \quad (36)$$

In the pressure shift model, Langmuir coefficients depend on the lattice molar volume, and we take that into account via the product and chain rules in accordance with Eq. (4) and Fig. 3.

$$\mu_w^{H} = \frac{\partial A^{EL}}{\partial N_w} + k_B T\left(\sum_j\left[\nu_j \ln\left(1-\sum_i\left[\Theta_{ij}\right]\right)\right]\right) + k_B T\left(\sum_j\left[N_w\nu_j\frac{\partial \ln\left(1-\sum_i\left[\Theta_{ij}\right]\right)}{\partial N_w}\right]\right) \quad (37)$$

Then, a contribution arises, which is equivalent to the pressure shift contribution ΔP^{H-EL}; in a *per mol* basis:

$$\Delta\mu_w^{H-EL} = \mu_w^{H} - \mu_w^{EL} = RT\left(\sum_j\left[\nu_j \ln\left(1-\sum_i\left[\Theta_{ij}\right]\right)\right]\right) + \Delta P^{H-EL}\overline{V}^{EL} \quad (38)$$

This expression allows us to calculate the chemical potential of water in the hydrate relative to the empty lattice condition. In order to perform phase equilibrium calculations we need to model the chemical potential of the empty lattice relative to a practical reference state: pure liquid water, conventional ice, or pure ideal gas.

Now, consider the case where C_{ij} and R_j were considered depending on $\overline{V}^{EL}$ through our geometry consideration, while the actual lattice volume was considered independent of pressure ($k \approx 0$). In this case, we are in a consistent *limit case* where our model, despite the pressure shift, yields the same results for chemical potential of hydrate with respect to pure water as the *standard* model with constant volume. This happens because the new contribution in the $\Delta\mu^{H-EL}$ expression ($\overline{V}^{EL}\Delta P^{H-EL}$) cancels out with the new contribution arising in $\Delta\mu^{EL-PW}$: the difference between the Poynting integral in the *standard* model and the *pressure shift* model lies in the upper limit of integration; in the former case, the upper limit was $P^{EL} = P^{H}$ and, now it is $P^{EL} = P^{H} - \Delta P^{H-EL}$; therefore the difference between the Poynting integral of a constant $\overline{V}$ from one case to the other is the same ($\overline{V}^{EL}\Delta P^{H-EL}$) factor.

1.7.4. *Internal energy and enthalpy*

We note that our modification influence the enthalpy calculations previously presented by a few works [29, 30, 11]. This property appears in the numerator for the Clapeyron equation, therefore it is related to the slope of the equilibrium curve, besides being fundamental for energy balances in general.

The derivation for enthalpy begins with the relation between internal energy and the partition function, according to:

$$U^{\mathrm{H}} = -k_{\mathrm{B}}T^2\left(\frac{\partial \Psi/k_{\mathrm{B}}T}{\partial T}\right)_{V^{\mathrm{H}},N_{\mathrm{w}},\underline{\lambda}} \tag{39}$$

where, as in the pressure calculation, a contribution from the empty lattice partition (Q^{EL}) function arises, and it leads to the internal energy of the empty lattice (U^{EL}) at given T, V, N_{w}, whereas, from q_{ij}, Φ_i leads to the intensive internal energy of an ideal gas at that temperature $\overline{U}^{IG}$

The internal energy of the hydrate can be expressed relatively to the internal energy of the empty lattice at a same T, V, N_{w} by

$$\frac{U^{\mathrm{H}} - U^{\mathrm{EL}} - \sum_i N_i^{\mathrm{g}}\overline{U}^{\mathrm{IG}}}{N_{\mathrm{w}}k_{\mathrm{B}}T^2} = \sum_i\sum_j\left[\nu_j\Theta_{ij}\left(\frac{\partial \ln\left(TC_{ij}\right)}{\partial T}\right)\right] \tag{40}$$

From that, we can derive enthalpy using

$$H^{\mathrm{H}} = U^{\mathrm{H}} + P^{\mathrm{H}}V^{\mathrm{H}} \tag{41}$$

$$H^{\mathrm{EL}} = U^{\mathrm{EL}} + P^{\mathrm{EL}}V^{\mathrm{EL}} \tag{42}$$

$$\overline{H}^{\mathrm{IG}} = \overline{U}^{\mathrm{IG}} + k_{\mathrm{B}}T \tag{43}$$

where $V = V^{\mathrm{H}} = V^{\mathrm{EL}}$ but $P^{\mathrm{H}} = P^{\mathrm{EL}} + \Delta P^{\mathrm{H-EL}}$, therefore

$$\begin{aligned}\frac{\Delta H^{\mathrm{H-EL-IG}}}{N_{\mathrm{w}}} = \frac{H^{\mathrm{H}} - H^{\mathrm{EL}} - \sum N_i\overline{H}^{\mathrm{IG}}}{N_{\mathrm{w}}} = \\ +\overline{V}^{\mathrm{EL}}\Delta P^{\mathrm{H-EL}} - k_{\mathrm{B}}T\frac{\sum_i N_i}{N_{\mathrm{w}}} \\ + k_{\mathrm{B}}T^2\sum_i\sum_j\left[\nu_j\Theta_{ij}\left(\frac{\partial \ln\left(TC_{ij}\right)}{\partial T}\right)\right]\end{aligned} \tag{44}$$

This expression represents the enthalpy of adsorption of molecules of guest component on an empty lattice, from an ideal gas phase, per molecule of water.

1.8. *Summary of modeling*

In this paper, we propose a new model called the *Pressure Shift* (PShift) model and compare its assumptions with three other models which we call *Standard*, *Interstitial* and *Inconsistent*. In this section, we try to summarize the differences discussed; these four classes of the van der Waals and Platteeuw model differ from one to another by combining assumptions in different manners, thus considering some phenomena and neglecting others, the consequences are illustrated in Fig. 4:

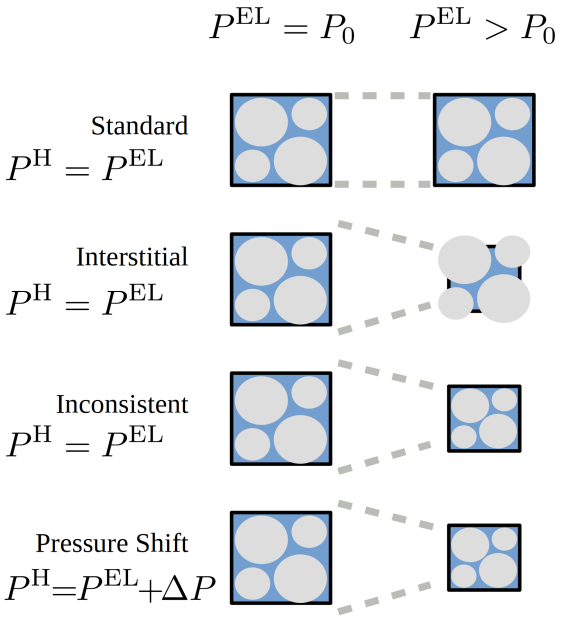

Figure 4: Comparison of different lattice behavior modeled in literature (Standard, Interstitial and Inconsistent) and proposed here (Pressure shift).

The standard modeling approach is the van der Waals and Platteeuw model assuming constant cages radii and constant molar volume; e.g. [23, 26, 27].

The modeling approach we call interstitial assumes possible variations of volume with temperature and lattice pressure but neglects variations of cage radius and this affects the Poynting integrals. However, because cages radii remains constant, this does not affecting Langmuir coefficients and does not result in a pressure shift contribution; e.g. [10, 11].

The modeling approach we labeled as inconsistent refers to a family of models that use Langmuir coefficients dependent on molar volume, without revising the expressions for derived properties; e.g. [5, 16]. Molar volume and cages radii vary with temperature and pressure, but the $\Delta P^{\mathrm{H-EL}}$ contribution is not acknowledged, and consequently, the hydrate pressure P^{H} is assumed to be equal to the reference lattice pressure P^{EL}. They are labeled inconsistent for failing to pass the Clapeyron equation test, as illustrated in Fig 7.

The pressure shift model is the approach proposed here, in which revising the expressions for derived properties, we showed a difference between the pressure of the actual clathrate and that of the empty lattice having the same volume, and this yielded new contributions in the expressions for several thermodynamic properties, as shown.

1.9. Pressure shift solution algorithm

We have stated that our model has, intrinsically, an interdependence in the variables Θ_{ij}, $\overline{V}^{\mathrm{EL}}$ R_j, $\Delta P^{\mathrm{H-EL}}$, P^{H}, and P^{EL} (Equation 3). In a simplest case, given a value for the empty lattice pressure and fugacities of all guest components, the calculation of the pressure shift $\Delta P^{\mathrm{H-EL}} + P^{\mathrm{EL}}$ is straightforward, using `calcPShift`$(T, P^{\mathrm{EL}}, \hat{f}[:])$ (Fig. 5).

Function `calcPShift`$(T,\ P^{\mathrm{EL}},\ \hat{f}[:])$**:**

- `/* Calculate lattice molar volume: */`
- $\overline{V}^{\mathrm{EL}} =$ `f_VEL` $\left(T, P^{\mathrm{EL}}\right)$ `// (Eq. 26)`
- `/* Calculate cages radii: */`
- $R[:] =$ `f_R` $\left(\overline{V}^{\mathrm{EL}}\right)$ `// (Eq. 23,21,19)`
- `/* Calculate Langmuir coefficients: */`
- $C[:,:] =$ `f_CLang` (T, R) `// (Eq. 17)`
- `/* Calculate occupancies: */`
- $\Theta[:,:] =$ `f_Occ` $\left(C, \hat{f}\right)$ `// (Eq. 30)`
- `/* Calculate CLang derivatives: */`
- $\mathrm{dC}_{dV}[:,:] =$ `f_dCdVEL` (T, R) `// (Eq. 25)`
- `/* Calculate the pressure shift: */`
- $\Delta P^{\mathrm{H-EL}} =$ `f_DPHEL` $(T, \Theta, \mathrm{dC}_{dV})$ `// (Eq. 35)`
- **return** $\Delta P^{\mathrm{H-EL}}$

Figure 5: Pressure shift calculation

Then the hydrate pressure is calculated from $P^{\mathrm{H}} = \Delta P^{\mathrm{H-EL}} + P^{\mathrm{EL}}$. However, for direct specification of P^{H}, an iterative solution method is required. We developed the successive substitution algorithm `convergePEL` $\left(T, P^{\mathrm{H}}, \hat{f}[:]\right)$ (Fig. 6) to converge the pressure shift and obtain thermodynamic properties of the hydrate.

Function `convergePEL`$(T,\ P^{\mathrm{H}},\ \hat{f}[:])$**:**

- `/* Guess a null pressure shift: */`
- $\Delta P^{\mathrm{H-EL}} = 0$
- **do**
  - `/* Calculate the lattice pressure: */`
  - $P^{\mathrm{EL}} = P^{\mathrm{H}} - \Delta P^{\mathrm{H-EL}}$
  - `/* Update the pressure shift: */`
  - $\Delta P^{\mathrm{H-EL}} =$ calcPShift$(T, P^{\mathrm{EL}}, \hat{f}[:])$
  - `/* Calculate the residue: */`
  - $\mathrm{RES} = \left(\left[\Delta P^{\mathrm{H-EL}}\right]^{k+1} - \left[\Delta P^{\mathrm{H-EL}}\right]^{k}\right) / P^{\mathrm{H}}$
- **loop while** abs $(\mathrm{RES}) > 1 \times 10^{-9}$;
- `/* Calculate the lattice pressure: */`
- $P^{\mathrm{EL}} = P^{\mathrm{H}} - \left[\Delta P^{\mathrm{H-EL}}\right]^{*}$
- **return** P^{EL}

Figure 6: Lattice pressure convergence algorithm

1.10. The Clapeyron equation as a consistency check

Previous works have considered the dependence of R_j with $\overline{V}$ in the Langmuir coefficients calculations while not considering the pressure shift in $\Delta\mu^{\mathrm{H-EL}}$ or $\Delta\mu^{\mathrm{EL-PW}}$ expressions. Here, we show this leads to an inconsistency noticeable in phase equilibrium calculations. According to the multicomponent and multiphase expression for the Clapeyron equation for univariant equilibrium [31, 9],

$$\frac{\mathrm{d}P}{\mathrm{d}T} = \frac{|\Delta\overline{H}^{\mathrm{uni}}|}{T|\Delta\overline{V}^{\mathrm{uni}}|} = \frac{\begin{vmatrix} -\overline{H}^{\mathrm{H}}/T^2 & x_{\mathrm{w}}^{\mathrm{H}} & x_{\mathrm{g}}^{\mathrm{H}} \\ -\overline{H}^{\mathrm{Pw}}/T^2 & x_{\mathrm{w}}^{\mathrm{Pw}} & x_{\mathrm{g}}^{\mathrm{Pw}} \\ -\overline{H}^{\mathrm{G}}/T^2 & x_{\mathrm{w}}^{\mathrm{G}} & x_{\mathrm{g}}^{\mathrm{G}} \end{vmatrix}}{\begin{vmatrix} -\overline{V}^{\mathrm{H}}/T & x_{\mathrm{w}}^{\mathrm{H}} & x_{\mathrm{g}}^{\mathrm{H}} \\ -\overline{V}^{\mathrm{Pw}}/T & x_{\mathrm{w}}^{\mathrm{Pw}} & x_{\mathrm{g}}^{\mathrm{Pw}} \\ -\overline{V}^{\mathrm{G}}/T & x_{\mathrm{w}}^{\mathrm{G}} & x_{\mathrm{g}}^{\mathrm{G}} \end{vmatrix}} \tag{45}$$

where G means the guest component fluid phase, either as Vapor or Liquid. Considering the common approximation of $x_{\mathrm{w}}^{\mathrm{G}} = 0$ and $x_{\mathrm{g}}^{\mathrm{Pw}} = 0$, it simplifies to

$$\Delta\overline{V}^{\mathrm{uni}} = \overline{V}^{\mathrm{H}} - \overline{V}^{\mathrm{Pw}} x_{\mathrm{w}}^{\mathrm{H}} - \overline{V}^{\mathrm{G}} x_{\mathrm{g}}^{\mathrm{H}} \tag{46}$$

$$\Delta\overline{H}^{\mathrm{uni}} = \overline{H}^{\mathrm{H}} - \overline{H}^{\mathrm{Pw}} x_{\mathrm{w}}^{\mathrm{H}} - \overline{H}^{\mathrm{G}} x_{\mathrm{g}}^{\mathrm{H}} \tag{47}$$

which are the variations in volume and enthalpy, respectively, on the dissociation of 1 mol of hydrate into Pw and G; $\overline{V}^{\mathrm{H}} = V^{\mathrm{H}}/(N_{\mathrm{w}} + \sum_i N_i^{\mathrm{g}})$ and $\overline{H}^{\mathrm{H}} = H^{\mathrm{H}}/(N_{\mathrm{w}} + \sum_i N_i^{\mathrm{g}})$.

As the slope (dP/dT) is equal to the ratio between $|\Delta H^{\mathrm{uni}}|$ and $T|\Delta\overline{V}^{\mathrm{uni}}|$, when $|\Delta\overline{V}^{\mathrm{uni}}|$ vanishes, the phase equilibrium curve has vertical slope.

Here, we show the application of this test to the phase equilibrium diagram of hydrate of an arbitrary pseudo component as illustrated in Fig. 7.

The continuous curves are the Pressure $\times$ Temperature phase equilibrium locus. The dotted curves are the contour level for the relation $|\Delta\overline{V}^{\mathrm{uni}}| = 0$. The black curves and dark gray curves represent the standard and the interstitial models, respectively, both of which meet this Clapeyron equation criterion. While, as shown in light gray, a model Langmuir coefficients dependent on lattice volume lacks this consistency if the derived properties equations are not revised. Finally, the red curve results from the Pressure-shift model proposed here.

In summary, the inclusion of volume-dependent Langmuir coefficients achieves a sensitivity of the phase equilibrium behavior regarding the model parameters at high pressure, as previously noted. The revision of expressions, in turn, ensures that the model passes the Clapeyron equation consistency test and achieves a sensitivity of the phase equilibrium behavior regarding the model parameters also at low pressure, this last feature

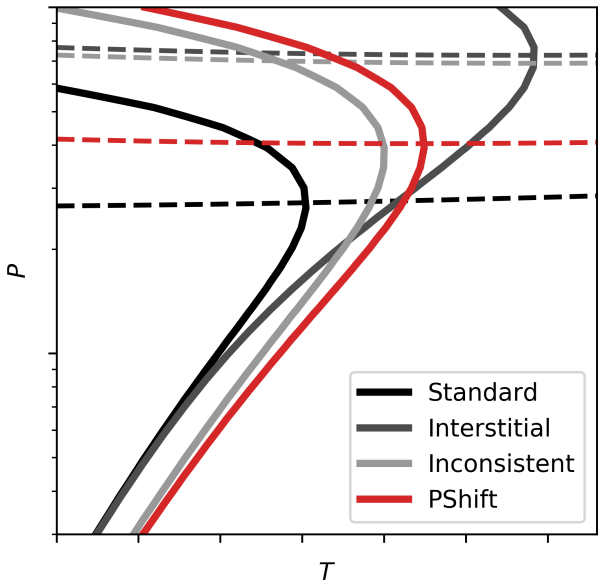

Figure 7: Consistency test with the Clapeyron equation: solid curves are phase equilibrium loci for each model, dashed curves are the loci of null molar volume determinant. (—) the black curves represent the *Standard* model, (—) the dark gray curves represent the *Interstitial* model, (—) the light gray curves represent the *Inconsistent* model, (—) the red curves represent the *Pressure Shift* (PShift) model. If a given model has thermodynamic consistency, the null molar volume determinant curve intercepts the point of the phase equilibrium loci where the slope is vertical.

mainly being a consequence of the volume and cages radii changes due to the guest-host interaction at low bulk pressure.

2. Phase Equilibrium Framework

2.1. Phase equilibrium calculations

We have performed phase equilibrium calculations for the 3-phase curve: hydrate s$^{\mathrm{I}}$+ liquid water + gas or liquid guests. For these phase equilibrium calculations we have solved the criterion given by

$$\Delta\mu_{\mathrm{w}}^{\mathrm{H-EL}} + \Delta\mu_{\mathrm{w}}^{\mathrm{EL-Pw}} = 0 \tag{48}$$

where $\Delta\mu^{\mathrm{EL-Pw}}$ is the difference in chemical potential of the empty lattice at pressure P^{EL} and stable pure water at system pressure P (ice or liquid).

The chemical potential of the empty lattice in $\Delta\mu^{\mathrm{EL-Pw}}$ is expressed not from an actual empty lattice partition function model but rather as four contributions: $\Delta\mu_0^{\mathrm{EL-Pw}}$, a chemical potential difference taken at T_0 and P_0; $\overline{V}^{\mathrm{EL}}$, a correlation for the molar volume of the empty lattice as a function of T and P^{EL}; $\overline{V}^{\mathrm{Pw}}$, a correlation for the molar volume of the stable pure water as a function of T and P; and $\Delta\overline{H}_0^{\mathrm{EL-Pw}}$, the molar enthalpy difference between the empty lattice and the stable pure water at P_0, as a function of T. The resulting expression, with all properties in *per mol* basis, is

$$\frac{\Delta\mu^{\mathrm{EL-Pw}}}{RT} = \frac{\Delta\mu_0^{\mathrm{EL-Pw}}}{RT_0} - \int_{T_0}^{T} \frac{\Delta\bar{H}_0^{\mathrm{EL-Pw}}}{RT^2}\mathrm{d}T + \int_{P_0}^{P^{\mathrm{EL}}} \frac{\bar{V}^{\mathrm{EL}}}{RT}\mathrm{d}P - \int_{P_0}^{P} \frac{\bar{V}^{\mathrm{Pw}}}{RT}\mathrm{d}P \tag{49}$$

We note that our equation expresses the difference in chemical potential for the host molecule at given T, P^{EL}, and N_{w} in empty lattice condition to a stable pure water condition at system pressure P. We deal separately with expressions for molar volume of the empty lattice and the stable pure water.

We also emphasize that the upper limit pressure in the Poynting integral of the empty lattice (second to the last term in Eq. 49) must consistently match P^{EL} from Eq. 13 throughout derivation and implementation. It is important to point this out because our model shows that the pressure associated with the empty lattice P^{EL} in thermodynamic properties and phase equilibrium calculations is different from the actual hydrate pressure, which is the system pressure. While current literature relies on $P^{\mathrm{H}} = P^{\mathrm{EL}}$.

For phase equilibrium calculations with either a gas or liquid phase rich in guest components, we used the Peng and Robinson equation of state [32] to calculate guest fluid phase fugacities: in the chemical equilibrium criterion of guests species, the fugacity for each guest type i in the fluid phase is equal to the fugacity of that guest type i associated with any cage type j in the hydrate phase.

$$\hat{f}_i^{\mathrm{G}} = \hat{f}_{ij}^{\mathrm{H}} \tag{50}$$

The liquid water molar volume was calculated from a correlation based on experimental data of [33] and [34].

2.2. Enthalpy of dissociation

In order to obtain a practical application for the hydrate enthalpy expression derived here, we combine it with residual gas enthalpy at T, P, N_i, ($\Delta H^{\mathrm{G-IG}}$) and enthalpy of transformation for the lattice at T, P^{EL}, N_{w} into stable pure liquid water at T, P, N_{w} ($\Delta H^{\mathrm{EL-Pw}}$), resulting in an expression for the enthalpy of dissociation ($\Delta H^{\mathrm{G+Pw-H}}$). This combination is done weighting the terms with the composition into

$$\frac{\Delta H^{\mathrm{G+Pw-H}}}{N_{\mathrm{w}}} = -\frac{\Delta H^{\mathrm{H-EL-IG}}}{N_{\mathrm{w}}} + \sum_i \left[\frac{N_i}{N_{\mathrm{w}}}\Delta\overline{H}^{\mathrm{G-IG}}\right] + \Delta\overline{H}^{\mathrm{EL-Pw}} \quad (51)$$

This is analogous to the expression presented in [11], but noting, now, that $\Delta H^{\mathrm{EL-Pw}}$ represents a difference in enthalpy of an empty lattice at P^{EL} and a stable pure liquid water at P, and that $\Delta H^{\mathrm{H-EL-IG}}$ includes a pressure shift contribution ($\overline{V}^{\mathrm{EL}}\Delta P^{\mathrm{H-EL}}$).

The contribution of $\Delta H^{\mathrm{EL-PW}}$ can be expressed relative to a standard condition at T_0 and P_0 as

$$\begin{aligned}\Delta\overline{H}^{\mathrm{EL-Pw}} = \Delta\overline{H}_0^{\mathrm{EL-Pw}} &+ \int_{T_0}^{T} \Delta c_{P,0}{}^{\mathrm{EL-Pw}}\mathrm{d}T \\ &+ \int_{P_0}^{P^{\mathrm{EL}}} \left[\overline{V}^{\mathrm{EL}} - T\left(\frac{\partial\overline{V}^{\mathrm{EL}}}{\partial T}\right)_{P,N_{\mathrm{w}}}\right]\mathrm{d}P \\ &- \int_{P_0}^{P} \left[\overline{V}^{\mathrm{Pw}} - T\left(\frac{\partial\overline{V}^{\mathrm{Pw}}}{\partial T}\right)_{P,N_{\mathrm{w}}}\right]\mathrm{d}P \quad (52)\end{aligned}$$

As we noted in the expression for the chemical potential of water, in the limit case of constant lattice volume, the *PShift* model also yields the same results as the *standard* model for enthalpy calculations. If $\overline{V}^{\mathrm{EL}}$ was constant with respect to T and P, then the pressure shift contribution in the expression for $\Delta H^{\mathrm{H-EL-IG}}$ would be equal to the factor removed from the volume integral for enthalpy in the expression for the $\Delta H^{\mathrm{EL-PW}}$.

3. Results and discussion

We have applied our model to single hydrates of three components: methane, ethane, and xenon. We discuss the behavior captured by the model and the variation of that behavior from guest to guest (different interaction parameters). We compare the model results with available experimental data for phase equilibrium conditions and for volumetric information given as unit cell edge length.

All calculations of thermodynamic properties and phase equilibrium presented in this work were performed in the IPython environment for interactive computing [35], using the SciPy ecosystem of open-source software for mathematics, science, and engineering to handle data arrays [NumPy: 36], established numerical methods [SciPy: 37], and plots for both interactive data visualization and publication [Matplotlib: 38].

3.1. Parameterization of hydrate properties

We have tuned the hydrate framework parameters (unit cell, empty lattice formation, and guest enclathration), starting from tabulated values [39]. We used data for Pressure × Temperature of phase equilibrium from the NIST hydrate database and volumetric data from several references [7, 2, 8, 3, 4, 6], including empty lattice simulations from Belosludov et al. [28]. The optimal parameters, as reported here, provided a good representation of $P \times T$ phase equilibrium data in the pshift framework and a qualitative representation of volumetric data for the three single guest hydrates studied here.

We have use an adaptation of the approach presented in Medeiros et al. [11] for the parameter tuning. We have used an objective function with a contribution for phase equilibrium data added for datasets of single hydrates of each guest into a joint minimization and a contribution for volumetric data of single hydrates of each guest, by means of the edge length of the unit cell, with empirically chosen weights.

Table 1 lists all regression parameters related to the unit cell volume dependence on pressure and temperature, all regression parameters related to the scaling of the cage radius with the edge length, and some structural constants ($\underline{Z}$, $\underline{\nu}$, and $N_{\mathrm{w}}^{\mathrm{uc}}$). We emphasize that these parameters are associated directly to the empty lattice and applies to hydrates of all three tested components, where different edge lengths and cages radii and different apparent compressibility and expansivity are calculated due to the effects of the pressure shift.

Table 1: Empty lattice structure parameters

Unit Cell	s^{I}	
$a_{\mathrm{uc},0}$/Å	11.78	
α_1	1.494×10^{-4}	
α_2	1.415×10^{-6}	
k/Pa^{-1}	1.967×10^{-10}	
$N_{\mathrm{w}}^{\mathrm{uc}}$	46	
Cages	**Small**	**Large**
$R_{j,0}$/Å	3.904	4.038
k_{Rj}/Pa^{-1}	1.453×10^{-10}	3.483×10^{-11}
Z_j	20	24
ν_j	2/46	6/46

with $T_{\mathrm{uc},0} = 0$ K and $P_{\mathrm{uc},0} = 0$ Pa.

Table 2 lists all regression parameters related to the formation properties of the empty lattice, i.e., related to its chemical potential with respect to pure liquid water. We emphasize that these parameters are associated directly to the empty lattice at $P^{\mathrm{EL}} = P_0$, and are consistently used to model hydrates of all three tested components. They will, in practice, have different chemical potential relative to liquid water at bulk $P = P_0$ as a result of the different (shifted) lattice pressure associated with each of them at a given temperature and bulk pressure.

Table 2: Empty lattice formation parameters

	s^{I}
$\Delta\mu_0^{\mathrm{EL-Lw}}$ / J mol^{-1}	742.9
$\Delta\bar{H}_0^{\mathrm{EL-Lw}}$ / J mol^{-1}	−4089.5
$\Delta c_{P,0}{}^{\mathrm{EL-Lw}}$ / J mol^{-1} K	−12.39

with $T_0 = 273$ K and $P_0 = 1$ bar.

Table 3 lists all regression parameters related to the enclathration of guest molecules. These parameters work together with the fact that the cages radii change because of the pressure shift, so at any given temperature and pressure, a guest with effective size σ_i is interacting with a cage with radius $R_j(T, P^{\mathrm{EL}})$, where $P^{\mathrm{EL}} = P - \Delta P^{\mathrm{H-EL}}$.

Table 3: Kihara / Lennard-Jones and Devonshire guest parameters

	σ_i/Å	$(\epsilon_i/k_{\mathrm{B}})$/K
CH_4	3.595	127.4
C_2H_6	3.863	234.6
Xe	3.688	174.8

with all $a_i = 0$ Å.

In Table 3, σ_i and ϵ_i are combination parameters for the effective interaction between each guest i and water in the Lennard-Jones-Devonshire spherical approximation. The hard-core parameters a of the Kihara potential were set to zero, i.e., despite all equations having been derived for the kihara potential general case, the potential effectively used here was the Lennard-Jones potential.

3.2. *Empty lattice volume and guest dependent lattice volume*

According to the correlation used, the lattice volume $\overline{V}^{\mathrm{EL}}$ decreases as the lattice pressure P^{EL} increases and it increases as the temperature increases. The behavior for the empty lattice as a function of temperature and of lattice pressure is shown in Fig. 8a and Fig. 8b, respectively. The lines are temperature isopleths calculated at ambient pressure and zero pressure (indistinguishable) or pressure isopleths at two temperature levels: 20 K and 200 K. The markers are simulated data from references in these conditions, as noted in the legend [28]. Our curves agree moderately, but not quite well, to the empty lattice data because the tuning of parameters was done prioritizing actual hydrate volume and phase equilibrium data and the model in its current state was not able to quantitatively correlate all the available empty lattice and hydrate data simultaneously.

As the volume changes, also do the cages radii according to the proportionality criteria used. The behavior of radii with respect to the edge length as dictated by our proportionality criteria is given by the lines in Fig. 8c, while the round markers show the optimized mean-spherical-approximation radius and the associated edge length at $T_{\mathrm{uc},0} = 0$ K and $P_{\mathrm{uc},0} = 0$ Pa; in that figure, the square markers show the radius of each layer k of oxygen atoms that constitute each cage and the associated edge length, as measured for a hydrate of ethylene oxide by McMullan and Jeffrey (see the layers characterization in Ballard et al. [5] and atomistic coordinates in Takeuchi et al. [40]).

The behavior of Langmuir coefficients with respect to changes in radii depends on the relative size of the guest molecule and the cage. Therefore, each the guest molecule, having a different size, is subject to a different pressure shift and a different resulting volume of its single hydrate. The behavior of edge length for each of the guest molecules studied here is given as function of temperature in Fig. 8d at ambient pressure, and as a function of bulk pressure in Fig. 8e and Fig. 8f for $T = 271$ K and $T = 298$ K, respectively. Lines in blue, yellow, and green are calculated values for methane, ethane, and xenon, respectively. Markers in the same colors are experimental data from references noted in the legends [2, 7, 8, 4, 6, 3], dashed black lines are empty lattice edge length at given T and P^{EL} as calculated with the optimized parameters.

The calculations of edge length versus temperature at atmospheric pressure were performed at constant occupation Θ_{ij}, as given by the condition $(T, P, \underline{y})$ under which the hydrate sample was formed. That strategy was taken with the intention to represent the conditions under which these experiments were carried, as reported in the literature: the hydrate is first synthesized at a given temperature and pressure, from ice powder and in equilibrium with a pressurized guest fluid phase; then the samples are quenched, ground and sieved. Finally, the samples are brought to the experimental apparatus at atmospheric pressure where temperature is set to desired levels and measurements are taken [7, 8]. At this point, the samples are not anymore in contact with the guest fluid phases, but for a short duration presumably allowing negligible guest exchange with the environment.

In a plot of lattice size versus pressure for a given hydrates the pressure shift can be seen roughly as the horizontal difference between the lattice size curve for this hydrate and that for the empty lattice with the same volume - this observation has been discussed as the hydrate "effective pressure" in the lattice dynamics calculations of Belosludov et al. [28]. In the plots presented

here, all hydrate calculations yield edge lengths higher than that of the empty lattice at given T and P^{EL}. Therefore, all of these guests are causing expansion of the lattice in these conditions.

3.3. Phase equilibrium

We have compared the hydrate - liquid water - gas/liquid guest univariant phase equilibrium as calculated with the pressure shift model with experimental data, and with the other three modeling strategies described in Fig. 4.

In Figs. 9a, 9c, and 9e we show the phase equilibrium curve with optimal parameters compared to experimental data from several references obtained through the NIST hydrate viewer [41]. The parameter tuning provided good agreement with experimental data for phase equilibrium with liquid water - above 273 K. We have represented data ranging from around 10 bar up to 10 000 bar, including the retrograde dissociation region shown experimentally for methane and xenon single hydrates. The model predicts retrograde dissociation for ethane hydrates slightly above the highest pressure available in the data set. Experiments in that condition range should help validate the current state of the model, either by confirming the predictions or by helping improve the parameter set.

In Figs. 9b, 9d and 9f we show the phase equilibrium curve $\left(P^{\mathrm{H,G,Lw}} \times T\right)$ and the curve (locus) of null molar volume determinant $\left(\Delta\overline{V}^{\mathrm{uni}} = 0\right)$ in phase equilibrium diagrams for all 4 models for each of methane, ethane, and xenon, respectively. The comparison between models was performed using the parameters optimized to the pressure shift model; that comparison was not done with the intention of assessing model accuracy, but rather of understanding the sensitivity of the phase equilibrium to the pressure shift contribution with given parameters. We show the influence of each contribution on the phase equilibrium curve with given parameters, at both low and high pressure and on the null $\Delta\overline{V}^{\mathrm{uni}}$ line, which indicates consistency according to the Clapeyron equation. The colored curves show the pressure shift model for each guest with current parameters, while the curves in black, dark gray, and light gray show the results for the standard, interstitial and inconsistent models with current parameters, respectively, for the corresponding guest species.

The standard and interstitial models have constant cages radii; therefore, the adsorption is the same, and the chemical potential is very similar at low pressure; at high pressure, the curves for these models split because of the Poynting integral. The inconsistent and pressure shift have different cages radii than those at low pressure, mainly because in this comparison, the former two models use the cages radii taken at $T_{\mathrm{uc},0} = 0$ K as constant at all T, and the inconsistent model uses cages radii calculated according to T, therefore the properties for the latter two are different from those for the former two even at low pressure.

Nevertheless, the volume for the interstitial and inconsistent models are very similar, as they depend equally on temperature and pressure. The contour level for $|\Delta\overline{V}^{\mathrm{uni}}| = 0$ is only slightly different because of the slight difference in composition weighting, sometimes unnoticeable. Finally, the difference between the inconsistent and pressure shift models is due to the extent to which the guest distorts the lattice beyond intrinsic dependence on temperature and pressure.

For methane and xenon, relatively small molecules, the biggest influence of the model is at high pressure, where the lattice size changes significantly due to the intrinsic compressibility of the lattice, and predictions are very sensitive to considering or not this deformation in the lattice, and in the cages radii; the equilibrium curve is similar for the pressure shift and the inconsistent model. In the case of ethane, as it is a larger molecule, there is a stronger pressure shift, even at ambient bulk pressure, so the volume, cages radii, and equilibrium curves are all significantly different even then. In all cases, the difference in prediction of volume is rather different, so the locus for null molar volume determinant is different between these models, and in the case of the inconsistent model, it does not match the maximum temperature for the phase equilibrium curve, as should according to the Clapeyron rule. The null volume difference contour occurs at a pressure above the upper limit of calculations performed here for ethane and xenon.

3.4. Thermodynamic properties along the phase equilibrium locus

In this section, we plot thermodynamic properties: $\Delta P^{\mathrm{H-EL}}$, $\overline{V}^{\mathrm{EL}}$, Θ_{ij}, and $\Delta\overline{H}^{\mathrm{uni}}$, along with the equilibrium points of the phase equilibrium curve calculated with the pressure shift model for single hydrates of each of these guest species.

Fig. 10 shows calculations for methane, Fig. 11 shows calculations for ethane, and Fig. 12 shows calculations for xenon. In every case, panel (a) shows the pressure shift calculated, in all cases seem here the pressure shift was positive, therefore lattice pressure is less than bulk pressure; the black dashed line shows the baseline of $\Delta P = 0$, for other conditions or parameterization, negative values could also be found. This effect on volume is shown in panel (b) for each case, hydrate volume at the lower lattice pressure (continuous colorlines) is higher than empty lattice volume would be at that bulk pressure (black dashed line): $V^{\mathrm{H}}(P^{\mathrm{H}} = P)$ is equal to $V^{\mathrm{EL}}(P^{\mathrm{EL}} = P^{\mathrm{H}} + \Delta P^{(-)})$ and greater than $V^{\mathrm{EL}}(P^{\mathrm{EL}} = P)$. A negative pressure shift, going below the dashed line in panel (a), would yield hydrate volume smaller than the empty lattice volume, below the dashed line in panel (b). The change in Occupancy along the phase equilibrium

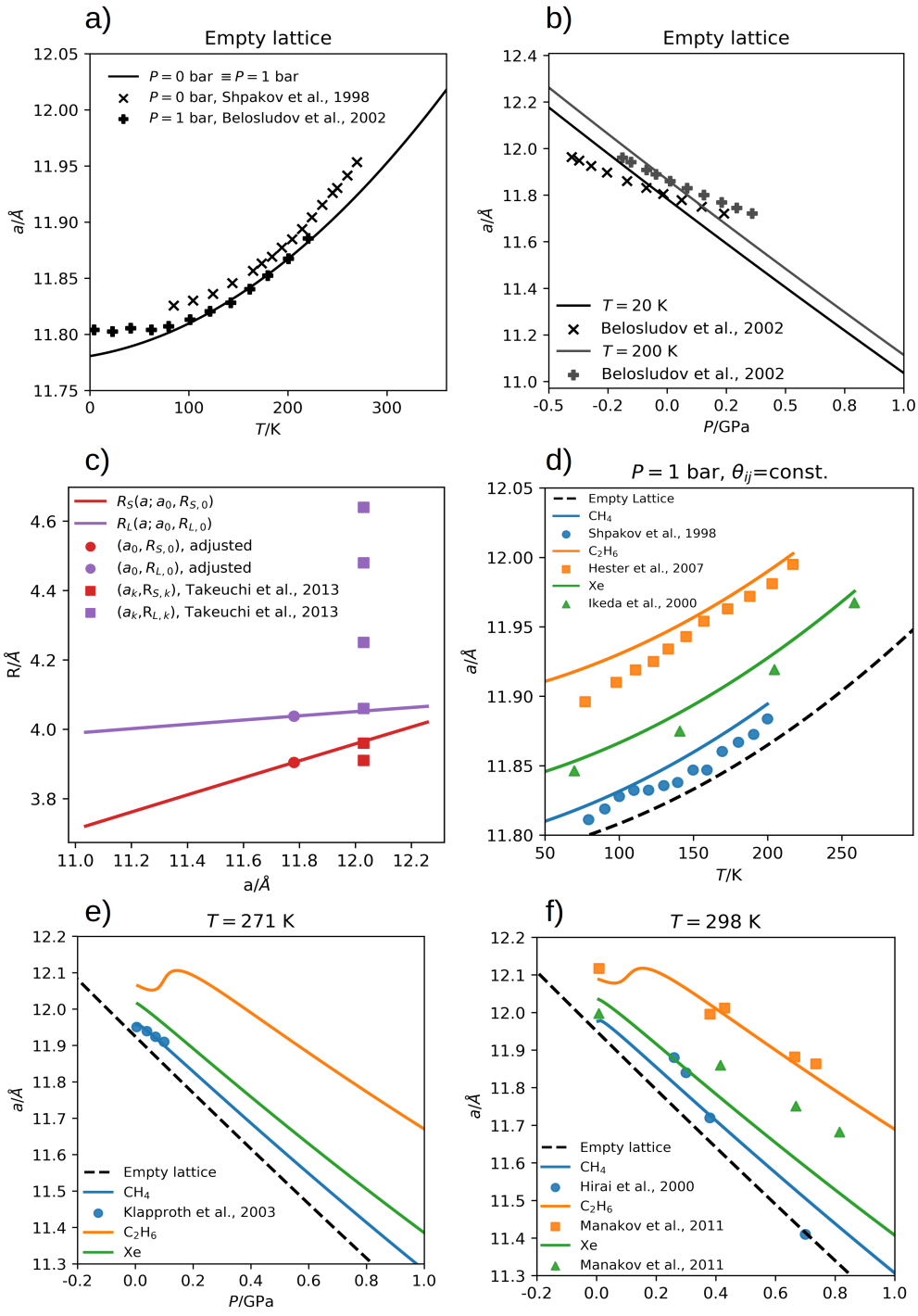

Figure 8: Volumetric data of s^I empty lattice and methane, ethane and xenon single hydrates: empty lattice unit cell edge length as function of T (a), empty lattice unit cell edge length as function ofP (b) cages radii as function of unit cell edge length (c) hydrate unit cell edge length as function of T for ambient pressure (d), hydrate unit cell edge length as function of P for T=271K (e), hydrate unit cell edge length as function of P for T=298K (f)

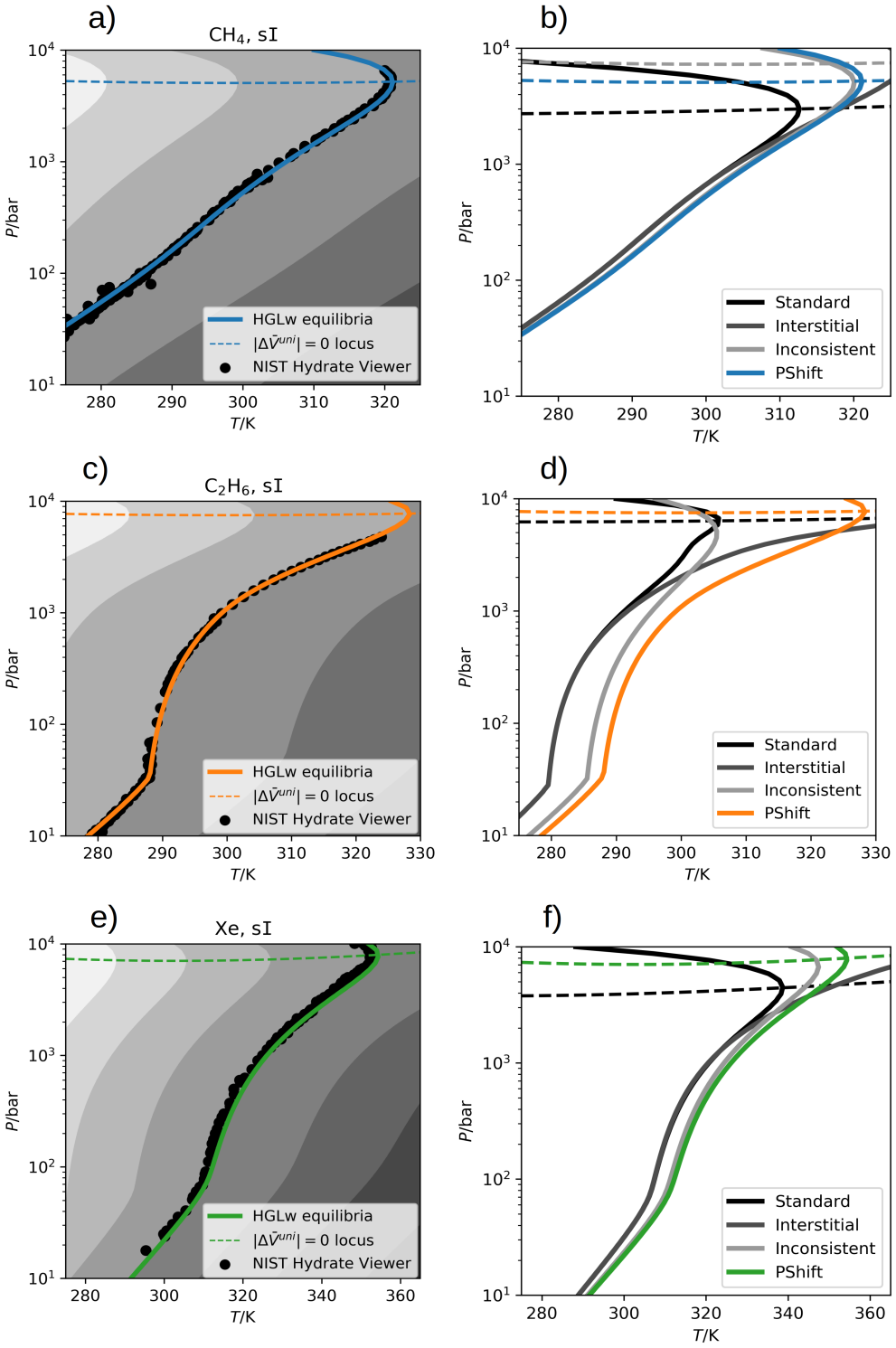

Figure 9: Phase equilibrium behavior of methane, ethane and xenon single hydrates. Optimized pressure shift model with experimental data (left) and comparison of contributions from each model variation (right)

locus is shown on panel (c) for each case: in all cases, the occupancy increases as pressure increases, albeit not necessarily in an obvious manner as each point that composes the curve is at a different temperature - the equilibrium temperature for that pressure, and as the fugacity is calculated from the equation of state. At last, panel (d), for all cases, show the dissociation enthalpy calculated with the pressure shift model, the full curves are the enthalpy of dissociation as defined in this text, while dashed and dotted are melting and desorption contributions, respectively (for interpretation purposes). The melting contribution is equivalent t the enthalpy of formation parameter, plus its contributions from the heat capacity difference and the Poynting-like integral of enthalpy ($\mathrm{d}\Delta H = \Delta C_P \mathrm{d}T + (\Delta\overline{V} - T\partial\Delta\overline{V}/\partial T)\mathrm{d}P$), the latter contribution makes the enthalpy of melting negative at very high pressure, as the liquid has lower molar volume than the empty lattice. The desorption contribution is associated with the interaction of guest molecules with the cages. It is calculated from derivatives of the Langmuir coefficients with respect to temperature and tends to increases in magnitude as occupancy increases, but is also related to the enthalpy of the fluid phase, which has a discontinuity when passing to a liquid-vapor transition pressure in the bulk phase, and continuous but not monotonical behavior slightly supercritical conditions (Joule-Thomson inversion phenomena).

Current calculations show very small occupancy of the small cage by ethane at low pressure, which is frequently assumed equal to zero [26]; however, they do predict that ethane enters the small cages at significant quantity for pressure above 1000 bar, along that the ethane hydrate has larger lattice size and cages radii than methane or xenon hydrates at the simulated conditions.

For ethane (Fig. 11), there are either cusps or discontinuities corresponding to liquid-vapor transition in all plots. The discontinuities happen for $\Delta\overline{H}^{\mathrm{uni}}$ because of the guest component fluid phase, which brings a contribution to the overall differences.

For Θ_{ij} and $\Delta P^{\mathrm{H-EL}}$, we obtain cusps because, as

$$\frac{\partial P^{\mathrm{H,Pw,G}}}{\partial T} = \frac{\Delta\overline{H}^{\mathrm{uni}}}{T\Delta\overline{V}^{\mathrm{uni}}} \tag{53}$$

A discontinuity in the right-hand side ratio is equivalent to a discontinuity in the left-hand side derivative and, consequently, the slope before and after the fluid phase transition is suddenly different.

The curves for Θ_{ij} and $\Delta P^{\mathrm{H-EL}}$ was calculated individually from each point in the phase equilibrium curve, but the curves for these properties must exactly correspond to the integration of

$$\left(\frac{\partial\Theta}{\partial P}\right)_{uni} = \left(\frac{\partial\Theta}{\partial T}\right)_{P}\left(\frac{\partial T}{\partial P}\right)_{uni} \tag{54}$$

and

$$\left(\frac{\partial\Delta P}{\partial P}\right)_{uni} = \left(\frac{\partial\Delta P}{\partial T}\right)_{P}\left(\frac{\partial T}{\partial P}\right)_{uni} \tag{55}$$

This shows how the cusp in the phase equilibrium curve given by $(\partial T/\partial P)_{uni}$ is propagated to the plots of Θ_{ij} and $\Delta P^{\mathrm{H-EL}}$ versus P^{H}.

For xenon, the critical point is slightly to the left of the phase equilibrium curve (lower T), so there is a change in the curvature of that curve, but without a cusp, this behavior is also observed in the properties shown here.

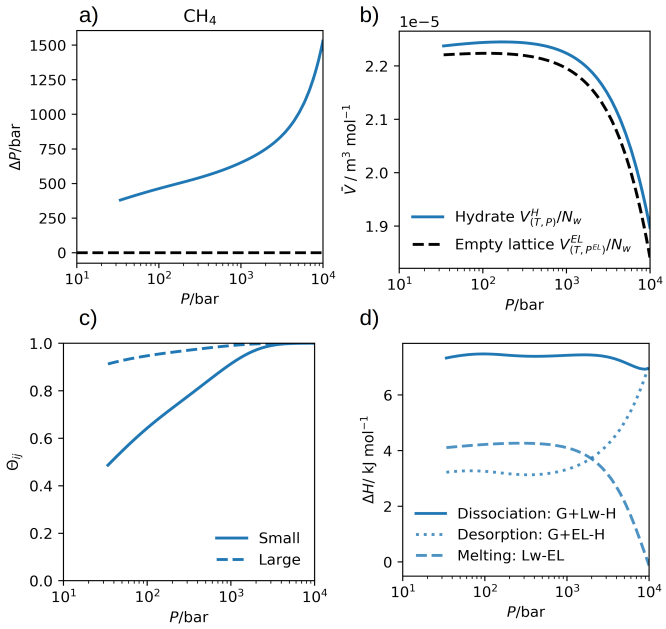

Figure 10: Thermodynamic properties of methane hydrate along the three phase (H,G,Lw) equilibrium locus: (a) pressure shift, (b) lattice volume, (c) occupancy, (d) enthalpy of dissociation

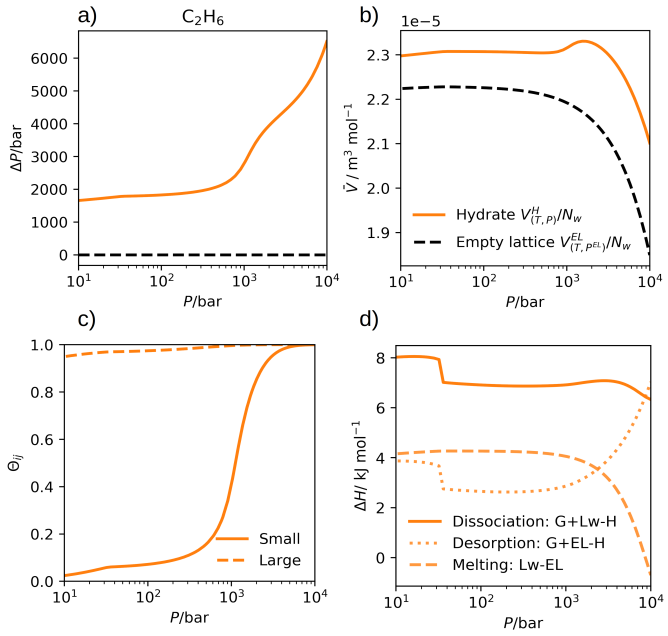

Figure 11: Thermodynamic properties of ethane hydrate along the three phase (H,G,Lw) equilibrium locus: (a) pressure shift, (b) lattice volume, (c) occupancy, (d) enthalpy of dissociation

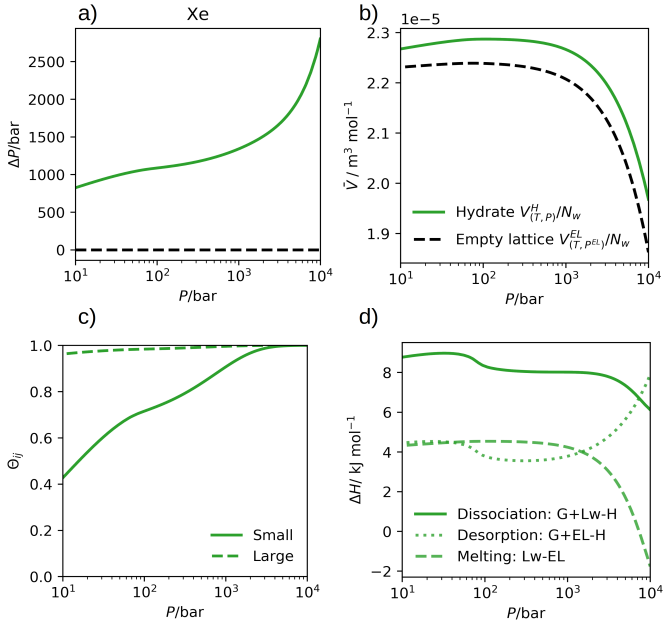

Figure 12: Thermodynamic properties of xenon hydrate along the three phase (H,G,Lw) equilibrium locus: (a) pressure shift, (b) lattice volume, (c) occupancy, (d) enthalpy of dissociation

4. Conclusions

This work reviewed thermodynamics of clathrates in the rigorous formulation based on the original van der Waals and Platteeuw model, where we have proposed an extension for compressible clathrates. Our extension of the van der Waals and Platteeuw model considers cages radii dependent on the clathrate volume, scaled according to the unit cell edge length, and obtains derived properties thermodynamically consistent with this assumption.

Our new formulation showed different volume for clathrates of different guests for the same structure at the same temperature and pressure, qualitatively in good agreement with experimental data. Furthermore, the phase equilibria are quantitatively in good agreement with experimental data. The proposed model solves a common thermodynamic inconsistency observed in phase equilibrium calculations using the state-of-the-art models for compressible clathrates.

We stress that our model extension does not require extra guest-dependent parameters other than the standard clathrate modeling framework. We have included only one set of parameters dependent on structure to tune the scaling of the cages radii with the edge length.

The proposed model is relevant for hydrate phase equilibrium at high pressure and for applications across a temperature range where changes in the volume are expected due to thermal expansivity. It is also relevant at low pressure in predicting volume and Langmuir coefficients of hydrates formed of different guests, where the pressure shift contribution from each guest type is different.

Acknowledgments

We would like to acknowledge and thank for the financial support from the Brazilian National Agency of Petroleum, Natural Gas and Biofuels (ANP, Brazil) and PETROBRAS through the Clause of Investments in Research, Development and Innovation. This study was also partially financed by the Coordination for the Improvement of Higher Education Personnel (CAPES, Brazil).

References

[1] J. Tse, Thermal expansion of the clathrate hydrates of ethylene oxide and tetrahydrofuran, Le Journal de Physique Colloques 48 (1987) C1–543. doi:10.1051/jphyscol:1987174.

[2] V. Shpakov, J. Tse, C. Tulk, B. Kvamme, V. Belosludov, Elastic moduli calculation and instability in structure i methane clathrate hydrate, Chemical Physics Letters 282 (1998) 107–114. doi:10.1016/S0009-2614(97)01241-4.

[3] A. Klapproth, E. Goreshnik, D. Staykova, H. Klein, W. F. Kuhs, Structural studies of gas hydrates, Canadian journal of physics 81 (2003) 503–518. doi:10.1139/p03-024.

[4] H. Hirai, T. Kondo, M. Hasegawa, T. Yagi, Y. Yamamoto, T. Komai, K. Nagashima, M. Sakashita, H. Fujihisa, K. Aoki, Methane hydrate behavior under high pressure, The Journal of Physical Chemistry B 104 (2000) 1429–1433. doi:10.1021/jp9926490.

[5] A. L. Ballard, E. D. Sloan Jr., The next generation of hydrate prediction: I. hydrate standard states and incorporation of spectroscopy, Fluid Phase Equilibria 194-197 (2002) 371–383. doi:10.1016/s0378-3812(01)00697-5.

[6] A. Y. Manakov, A. Y. Likhacheva, V. A. Potemkin, A. G. Ogienko, A. V. Kurnosov, A. I. Ancharov, Compressibility of gas hydrates, ChemPhysChem 12 (2011) 2476–2484. doi:10.1002/cphc.201100126.
[7] K. C. Hester, Z. Huo, A. L. Ballard, C. A. Koh, K. T. Miller, E. D. Sloan, Thermal expansivity for si and sii clathrate hydrates, The Journal of Physical Chemistry B 111 (2007) 8830–8835. doi:10.1021/jp0715880.
[8] T. Ikeda, S. Mae, O. Yamamuro, T. Matsuo, S. Ikeda, R. M. Ibberson, Distortion of host lattice in clathrate hydrate as a function of guest molecule and temperature, The Journal of Physical Chemistry A 104 (2000) 10623–10630. doi:10.1021/jp001313j.
[9] F. d. A. Medeiros, I. S. V. Segtovich, F. W. Tavares, A. K. Sum, Sixty years of the van der waals and platteeuw model for clathrate hydrates—a critical review from its statistical thermodynamic basis to its extensions and applications, Chemical Reviews 120 (2020) 13349–13381. doi:10.1021/acs.chemrev.0c00494.
[10] J. B. Klauda, S. I. Sandler, A fugacity model for gas hydrate phase equilibria, Industrial & engineering chemistry research 39 (2000) 3377–3386. doi:10.1021/ie000322b.
[11] F. d. A. Medeiros, I. S. V. Segtovich, A. G. Barreto Jr., F. W. Tavares, Heat of dissociation from statistical thermodynamics: Using calorimetric data to estimate gas hydrate parameters, The Journal of Chemical Thermodynamics 117 (2018) 164–179. doi:10.1016/j.jct.2017.08.005.
[12] M.-J. Hwang, G. D. Holder, S. R. Zele, Lattice distortion by guest molecules in gas-hydrates, Fluid Phase Equilibria 83 (1993) 437–444. doi:10.1016/0378-3812(93)87048-6.
[13] S. Zele, S.-Y. Lee, G. Holder, A theory of lattice distortion in gas hydrates, The Journal of Physical Chemistry B 103 (1999) 10250–10257. doi:10.1021/jp9917704.
[14] S.-Y. Lee, G. D. Holder, Model for gas hydrate equilibria using a variable reference chemical potential: Part 1, AIChE Journal 48 (2002) 161–167. doi:10.1002/aic.690480116.
[15] J. E. Lennard-Jones, A. Devonshire, Critical phenomena in gases 1, Proc. R. Soc. Lond. A 163 (1937) 53–70. doi:10.1098/rspa.1937.0210.
[16] M.-K. Hsieh, W.-Y. Ting, Y.-P. Chen, P.-C. Chen, S.-T. Lin, L.-J. Chen, Explicit pressure dependence of the langmuir adsorption constant in the van der waals–platteeuw model for the equilibrium conditions of clathrate hydrates, Fluid Phase Equilibria 325 (2012) 80–89. doi:10.1016/j.fluid.2012.04.012.
[17] I. S. V. Segtovich, A Non-Ideal Hydrate Solid Solution Model For A Multi-Phase Equilibria Program, Ph.D. thesis, Universidade Federal do Rio de Janeiro, 2018. URL: objdig.ufrj.br/61/teses/874275.pdf.
[18] M. Vandamme, Coupling between adsorption and mechanics (and vice versa), Current Opinion in Chemical Engineering 24 (2019) 12–18. doi:https://doi.org/10.1016/j.coche.2018.12.005, materials engineering: bio-derived/bio-inspired materials. Separations Engineering: advances in adsorption.
[19] K. Kulasinski, R. Guyer, D. Derome, J. Carmeliet, Poroelastic model for adsorption-induced deformation of biopolymers obtained from molecular simulations, Phys. Rev. E 92 (2015) 022605. doi:10.1103/PhysRevE.92.022605.
[20] L. Brochard, M. Vandamme, R.-M. Pellenq, Poromechanics of microporous media, Journal of the Mechanics and Physics of Solids 60 (2012) 606–622. doi:https://doi.org/10.1016/j.jmps.2012.01.001.
[21] Y. Zhang, Mechanics of adsorption–deformation coupling in porous media, Journal of the Mechanics and Physics of Solids 114 (2018) 31–54. doi:https://doi.org/10.1016/j.jmps.2018.02.009.
[22] P. I. Ravikovitch, A. V. Neimark, Density functional theory model of adsorption deformation, Langmuir 22 (2006) 10864–10868. doi:10.1021/la061092u.
[23] J. H. van der Waals, J. C. Platteeuw, Clathrate solutions, Advances in chemical physics (1959) 1–57. doi:10.1002/9780470143483.ch1.
[24] D. A. McQuarrie, Statistical Mechanics, Harper and Row: New York, 1976. ISBN: 978-0-07-016190-0.
[25] R. M. Pratt, A. L. Ballard, E. Sloan Jr, Beware of singularities when calculating clathrate hydrate cell potentials!, AIChE journal 47 (2001) 1897–1898. doi:10.1002/aic.690470820.
[26] W. R. Parrish, J. M. Prausnitz, Dissociation pressures of gas hydrates formed by gas mixtures, Industrial & Engineering Chemistry Process Design and Development 11 (1972) 26–35. doi:10.1021/i260041a006.
[27] V. McKoy, O. Sinanoğlu, Theory of dissociation pressures of some gas hydrates, The journal of chemical physics 38 (1963) 2946–2956. doi:10.1063/1.1733625.
[28] V. R. Belosludov, T. M. Inerbaev, O. S. Subbotin, R. V. Belosludov, J.-i. Kudoh, Y. Kawazoe, Thermal expansion and lattice distortion of clathrate hydrates of cubic structures i and ii, Journal of Supramolecular Chemistry 2 (2002) 453–458. doi:10.1016/S1472-7862(03)00072-8.
[29] A. Jäger, V. Vinš, R. Span, J. Hrubỳ, Model for gas hydrates applied to ccs systems part iii. results and implementation in trend 2.0, Fluid Phase Equilibria 429 (2016) 55–66. doi:10.1016/j.fluid.2016.08.027.
[30] D. Avlonitis, An investigation of gas hydrates formation energetics, AIChE journal 51 (2005) 1258–1273. doi:10.1002/aic.10374.
[31] J. W. Tester, M. Modell, Thermodynamics and its applications, Prentice-Hall international series in the physical and chemical engineering sciences, 3rd ed ed., Prentice Hall PTR, Upper Saddle River, N.J, 1997. ISBN:978-0-13-915356-3.
[32] R. C. Reid, J. M. Prausnitz, B. E. Poling, The properties of gases and liquids, McGraw Hill Book Co., New York, NY, 1987. ISBN: 978-0070116825.
[33] R. Hilbert, K. Tödheide, E. Franck, Pvt data for water in the ranges 20 to 600° c and 100 to 4000 bar, Berichte der Bunsengesellschaft für physikalische Chemie 85 (1981) 636–643. ISSN: 0005-9021.
[34] D. R. Lide (Ed.), CRC handbook of chemistry and physics: a ready-reference book of chemical and physical data, 86. ed ed., CRC Press, Boca Raton, 2005. ISBN:978-0-8493-0486-6.
[35] F. Pérez, B. E. Granger, IPython: a system for interactive scientific computing, Computing in Science and Engineering 9 (2007) 21–29. doi:10.1109/MCSE.2007.53.
[36] C. R. Harris, K. J. Millman, S. J. van der Walt, R. Gommers, P. Virtanen, D. Cournapeau, E. Wieser, J. Taylor, S. Berg, N. J. Smith, R. Kern, M. Picus, S. Hoyer, M. H. van Kerkwijk, M. Brett, A. Haldane, J. F. del Río, M. Wiebe, P. Peterson, P. Gérard-Marchant, K. Sheppard, T. Reddy, W. Weckesser, H. Abbasi, C. Gohlke, T. E. Oliphant, Array programming with NumPy, Nature 585 (2020) 357–362. doi:10.1038/s41586-020-2649-2.
[37] E. Jones, T. Oliphant, P. Peterson, et al., SciPy: Open source scientific tools for Python, 2001. URL: http://www.scipy.org/.
[38] J. D. Hunter, Matplotlib: A 2d graphics environment, Computing In Science & Engineering 9 (2007) 90–95. doi:10.1109/MCSE.2007.55.
[39] G. Holder, S. Zetts, N. Pradhan, Phase behavior in systems containing clathrate hydrates: a review, Reviews in chemical engineering 5 (1988) 1–70. doi:10.1515/REVCE.1988.5.1-4.1.
[40] F. Takeuchi, M. Hiratsuka, R. Ohmura, S. Alavi, A. K. Sum, K. Yasuoka, Water proton configurations in structures i, ii, and h clathrate hydrate unit cells, The Journal of Chemical Physics 138 (2013) 124504. doi:10.1063/1.4795499.
[41] K. Kroenlein, C. Muzny, Diky, K. A. , V. Diky, R. Chirico, E. Sloan, M. Frenkel, Clathrate hydrate physical property database, 2015. URL: http://gashydrates.nist.gov/HydrateViewer/.

Appendix A. Derivation of the pressure shift model

In this appendix, we present some details on the derivation of thermodynamics properties from the semi-grand canonical partition function, taking into consideration the dependence of the partition function for the single enclathrated molecule under an external field with respect to lattice molar volume.

Appendix A.1. Derivatives of occupancy

Similarly, we need expressions for derivatives of Θ_{ij} for the obtainment of the remaining derived properties; we take generic derivatives from Eq. 29.

$$\mathrm{d}\Theta_{ij} = \mathrm{d}\left(\frac{q_{ij}\lambda_{ij}}{\sum_k \left[q_{kj}\lambda_{kj}\right]+1}\right) \tag{A.1}$$

then

$$\begin{aligned}\mathrm{d}\Theta_{ij} = &\frac{\lambda_{ij}}{\sum_k \left[q_{kj}\lambda_{kj}\right]+1}\mathrm{d}q_{ij} \\ &- \frac{q_{ij}\lambda_{ij}}{\left(\sum_k \left[q_{kj}\lambda_{kj}\right]+1\right)^2}\sum_k\left[\lambda_{kj}\mathrm{d}q_{kj}\right] \\ &+ \frac{q_{ij}}{\sum_k \left[q_{kj}\lambda_{kj}\right]+1}\mathrm{d}\lambda_{ij} \\ &- \frac{q_{ij}\lambda_{ij}}{\left(\sum_k \left[q_{kj}\lambda_{kj}\right]+1\right)^2}\sum_k\left[q_{kj}\mathrm{d}\lambda_{kj}\right]\end{aligned} \tag{A.2}$$

whose terms can be grouped into

$$\begin{aligned}\mathrm{d}\Theta_{ij} = &\left(\Theta_{ij}\left(1-\sum_k \Theta_{kj}\right)\right)\mathrm{d}\ln q_{ij} \\ &+ \left(\Theta_{ij}\left(1-\sum_k \Theta_{kj}\right)\right)\mathrm{d}\ln \lambda_{ij}\end{aligned} \tag{A.3}$$

this equation will be most useful for derivatives at constant $\underline{\lambda}$, and using that from Eq. 18

$$\mathrm{d}\ln q_{ij} = \mathrm{d}\ln T + \mathrm{d}\ln \Phi + \mathrm{d}\ln C_{ij} \tag{A.4}$$

Appendix A.2. Derivatives of the Langmuir Coefficients

We need to calculate derivatives of the Langmuir coefficients with respect to volume, number of molecules of water, and temperature.

The differential form of the Langmuir coefficients with respect to volume and number of water molecules at a constant temperature is

$$\mathrm{d}C_{ij}(V^{\mathrm{H}}, N_{\mathrm{w}}) = \frac{\partial C_{ij}}{\partial V^{\mathrm{H}}}\mathrm{d}V^{\mathrm{H}} + \frac{\partial C_{ij}}{\partial N_{\mathrm{w}}}\mathrm{d}N_{\mathrm{w}} \tag{A.5}$$

However, as it is assumed that the Langmuir coefficients can be expressed solely as a function of lattice molar volume, this must be equivalent to

$$dC_{ij}\left(\frac{V^{\mathrm{H}}}{N_{\mathrm{w}}}\right) = \frac{\partial C_{ij}}{\partial\left(\frac{V^{\mathrm{H}}}{N_{\mathrm{w}}}\right)}\mathrm{d}\left(\frac{V^{\mathrm{H}}}{N_{\mathrm{w}}}\right) \tag{A.6}$$

where the differential form of the lattice molar volume with respect to volume and number of water molecules is

$$\mathrm{d}\left(\frac{V^{\mathrm{H}}}{N_{\mathrm{w}}}\right) = \frac{\partial\left(\frac{V^{\mathrm{H}}}{N_{\mathrm{w}}}\right)}{\partial V^{\mathrm{H}}}\mathrm{d}V^{\mathrm{H}} + \frac{\partial\left(\frac{V^{\mathrm{H}}}{N_{\mathrm{w}}}\right)}{\partial N_{\mathrm{w}}}\mathrm{d}N_{\mathrm{w}} \tag{A.7}$$

Therefore, executing the partial derivatives

$$d\left(\frac{V^{\mathrm{H}}}{N_{\mathrm{w}}}\right) = \left(\frac{1}{N_{\mathrm{w}}}\right)dV^{\mathrm{H}} + \left(\frac{-V^{\mathrm{H}}}{N_{\mathrm{w}}^2}\right)dN_{\mathrm{w}} \tag{A.8}$$

Using this relation, we show that the differential form of the Langmuir coefficients with respect to volume and number of moles as independent variables takes a simple form for numerical calculations as follows, depending on the partial derivative of the Langmuir coefficients with lattice molar volume.

$$\mathrm{d}C_{ij} = \frac{\partial C_{ij}}{\partial \overline{V}^{\mathrm{EL}}}\left(\frac{1}{N_{\mathrm{w}}}\mathrm{d}V^{\mathrm{H}} + \frac{V^{\mathrm{H}}}{-(N_{\mathrm{w}})^2}\mathrm{d}N_{\mathrm{w}}\right) \tag{A.9}$$

From this, we express the symbolic partial derivatives of Langmuir coefficients with respect to volume

$$\left(\frac{\partial C_{ij}}{\partial V^{\mathrm{H}}}\right)_{T,N_{\mathrm{w}}} = \left(\frac{\partial C_{ij}}{\partial \overline{V}^{\mathrm{EL}}}\right)_T \frac{1}{N_{\mathrm{w}}} \tag{A.10}$$

and with respect to number of water molecules

$$\left(\frac{\partial C_{ij}}{\partial N_{\mathrm{w}}}\right)_{T,V^{\mathrm{H}}} = \left(\frac{\partial C_{ij}}{\partial \overline{V}^{\mathrm{EL}}}\right)_T \frac{V^{\mathrm{H}}}{-(N_{\mathrm{w}})^2} \tag{A.11}$$

both depending on the partial derivative of the Langmuir coefficients with respect only to lattice molar volume.

The derivatives of Langmuir coefficients with respect to lattice molar volume is related to the derivatives of Langmuir coefficients with respect to cage radii according to

$$\left(\frac{\partial C_{ij}}{\partial \overline{V}^{\mathrm{EL}}}\right)_T = \left(\frac{\partial C_{ij}}{\partial R_j}\right)_T \left(\frac{\partial R_j}{\partial \overline{V}^{\mathrm{EL}}}\right) \tag{A.12}$$

From Eq. A.4

$$\left(\frac{\partial \ln q_{ij}}{\partial R_j}\right)_T = \frac{1}{C_{ij}}\left(\frac{\partial C_{ij}}{\partial R_j}\right)_T \tag{A.13}$$

We can evaluate $\left(\partial C_{ij}/\partial R_j\right)_T$ from Eq. 17 using the Leibniz rule for differentiation of integrals

$$\begin{aligned}\frac{\partial}{\partial x}\int_l^u f(t;x)dt = &f(u;x)\left(\frac{\partial u}{\partial x}\right) \\ &- f(l;x)\left(\frac{\partial l}{\partial x}\right) + \int_l^u \left(\frac{\partial f}{\partial x}\right)(t;x)dt\end{aligned} \tag{A.14}$$

with R_j for x, 0 for l, $R_j - a_i$ for u, and $4\pi r^2 e^{(-w_{ij}/k_{\mathrm{B}}T)}$ for f.

Then

$$\left(\frac{\partial l}{\partial x}\right) = \left(\frac{\partial 0}{\partial R_j}\right) = 0 \tag{A.15}$$

and

$$\left(\frac{\partial u}{\partial x}\right) = \left(\frac{\partial R_j - a_i}{\partial R_j}\right) = 1 \tag{A.16}$$

however w_{ij} at the boundary is undetermined with limit at infinity

$$\lim_{r \to R_j - a_i} \left(w_{ij}\right) \to \infty \tag{A.17}$$

therefore, the exponential factor, in the limit, is zero

$$f(l;x) = \lim_{w_{ij}\to\infty} \left(4\pi r^2 e^{\frac{-w_{ij}}{k_B T}}\right) \to 0 \tag{A.18}$$

Finally ,the derivatives in the third contribution are taken symbolically

$$\begin{aligned}\left(\frac{\partial f(t;x)}{\partial x}\right) &= \left(\frac{\partial}{\partial R_j}\right)\left(4\pi r^2 \exp\left(\frac{-w_{ij}(r;R_j)}{T}\right)\right) \\ &= \frac{-4\pi}{T} e^{\left(\frac{-w_{ij}}{k_B T}\right)} \left(\frac{\partial w_{ij}}{\partial R_j}\right) r^2 \end{aligned} \tag{A.19}$$

then

$$\left(\frac{\partial C_{ij}}{\partial R_j}\right) = \frac{\int_0^{R_j - a_i} \frac{-4\pi r^2}{k_B T}\left(\frac{\partial w_{ij}}{\partial R_j}\right) \exp\left(\frac{-w_{ij}(r)}{k_B T}\right) \mathrm{d}r}{k_B T} \tag{A.20}$$

Regarding derivatives with respect to temperature, from Eq. A.4

$$\left(\frac{\partial \ln q_{ij}}{\partial T}\right)_{R_j} = \frac{1}{C_{ij} T}\left(\frac{\partial C_{ij} T}{\partial T}\right)_{R_j} + \left(\frac{\partial \ln \Phi_i}{\partial T}\right) \tag{A.21}$$

we evaluate again from Eq. 17 using the Leibniz rule for differentiation of integrals.

In this case, as neither of the limits $R_j - a_i$ and 0 are functions of T at constant V^{H} and N_{w}.

$$\left(\frac{\partial C_{ij} T}{\partial T}\right)_{R_j} = \frac{1}{k_B} \int_0^{R_j - a_i} \left(4\pi r^2 e^{\frac{-w_{ij}}{k_B T}} \frac{-w_{ij}}{k_B} \frac{-1}{T^2}\right) dr \tag{A.22}$$

We evaluate the free volume integrals for all of C_{ij}, $\left(\partial C_{ij}/\partial R_j\right)_T$ and $\left(\partial C_{ij} T/\partial T\right)_{R_j}$ using the composite Simpson method.

Appendix A.3. Cage potential

We describe q_{ij} and C_{ij} using the cage potential derived from the Kihara pair interaction potential. The resulting expression for w_{ij} as given by [23, 26, 27]

$$\mathtt{D1} = \frac{a_i}{R_j} \tag{A.23}$$

$$\mathtt{D2} = 1 - r/R_j - \mathtt{D1} \tag{A.24}$$

$$\mathtt{D3} = 1 + r/R_j - \mathtt{D1} \tag{A.25}$$

$$\mathtt{DEL}(i) = \frac{1}{i}\left(\mathtt{D2}^{-i} - \mathtt{D3}^{-i}\right) \tag{A.26}$$

$$\mathtt{R1} = \sigma_i^{12}/R_j^{11} \tag{A.27}$$

$$\mathtt{R2} = \sigma_i^{6}/R_j^{5} \tag{A.28}$$

$$\mathtt{S1} = \mathtt{DEL}(10) + \mathtt{D1DEL}(11) \tag{A.29}$$

$$\mathtt{S2} = \mathtt{DEL}(4) + \mathtt{D1DEL}(5) \tag{A.30}$$

$$w_{ij} = \frac{2 Z_j \epsilon_i}{r}\left(\mathtt{R1S1} - \mathtt{R2S2}\right) \tag{A.31}$$

where a_i, σ_i, and ϵ_i are the parameters from the Kihara pair interaction potential of guest component (i) and a water molecule from the lattice. Mono-spaced symbols represent non physically meaningful quantities used for breaking equations into smaller terms.

The expression for $\left(\partial w_{ij}/\partial R_j\right)$ is obtained symbolically from the expressions above for w_{ij}

$$\mathtt{dD1dR} = -a_i/R_j^2 \tag{A.32}$$

$$\mathtt{dD3dR} = 1 - r/R_j^2 - \mathtt{dD1dR} \tag{A.33}$$

$$\mathtt{dDELdR}(i) = -\mathtt{D2}^{-i-1}\mathtt{dD2dR} + \mathtt{D3}^{-i-1}\mathtt{dD3dR} \tag{A.34}$$

$$\mathtt{dR1dR} = -11\left(\sigma_i/R_j\right)^{12} \tag{A.35}$$

$$\mathtt{dR2dR} = -5\left(\sigma_i/R_j\right)^{-6} \tag{A.36}$$

$$\begin{aligned}\mathtt{dS1dR} &= \mathtt{dDELdR}(10) + \mathtt{dD1dRDEL}(11) \\ &\quad + \mathtt{D1dDELdR}(11)\end{aligned} \tag{A.37}$$

$$\begin{aligned}\mathtt{dS2dR} &= \mathtt{dDELdR}(4) + \mathtt{dD1dRDEL}(5) \\ &\quad + \mathtt{D1dDELdR}(5)\end{aligned} \tag{A.38}$$

$$\begin{aligned}\left(\frac{\partial w_{ij}}{\partial R_j}\right) &= \frac{2 Z_j \epsilon_i}{r}\Big(\mathtt{dR1dRS1} - \mathtt{dR2dRS2} \\ &\quad + \mathtt{R1dS1dR} - \mathtt{R2dS2dR}\Big)\end{aligned} \tag{A.39}$$

Appendix A.4. Hydrate pressure shift

To go from Eq. 34 to Eq. 35, we need to apply the expressions for derivatives of occupancy A.3.

$$\Delta P^{\mathrm{H-EL}} = - k_B T \sum_j \left[\nu_j N_{\mathrm{w}} \left(\frac{\partial \ln\left(1 - \sum_i \Theta_{ij}\right)}{\partial V^{\mathrm{H}}}\right)_{T, N_{\mathrm{w}}, \underline{\lambda}}\right] \tag{A.40}$$

Taking the chain rule on the differentiation of the logarithm function

$$\Delta P^{\mathrm{H-EL}} = k_{\mathrm{B}}T\sum_j\left[\frac{\nu_j N_{\mathrm{w}}}{1-\sum_i\Theta_{ij}}\sum_i\left[\left(\frac{\partial\Theta_{ij}}{\partial V^{\mathrm{H}}}\right)_{T,N_{\mathrm{w}},\underline{\lambda}}\right]\right] \quad \text{(A.41)}$$

The derivatives of occupancy with respect to volume are taken from Eq. A.2.

$$\left(\frac{\partial\Theta_{ij}}{\partial V^{\mathrm{H}}}\right)_{T,N_{\mathrm{w}},\underline{\lambda}} = \left(\Theta_{ij}\left(1-\sum_k\Theta_{kj}\right)\right)\left(\frac{\partial\ln q_{ij}}{\partial V^{\mathrm{H}}}\right)_{T,N_{\mathrm{w}},\underline{\lambda}} \quad \text{(A.42)}$$

Then, on substitution

$$\Delta P^{\mathrm{H-EL}} = k_{\mathrm{B}}T\sum_j\left[\frac{\nu_j N_{\mathrm{w}}}{1-\sum_i\Theta_{ij}} \times\left(\sum_i\left[\Theta_{ij}\left(1-\sum_k\Theta_{kj}\right)\left(\frac{\partial\ln q_{ij}}{\partial V^{\mathrm{H}}}\right)_{T,N_{\mathrm{w}},\underline{\lambda}}\right]\right)\right] \quad \text{(A.43)}$$

This can be rearranged into

$$\Delta P^{\mathrm{H-EL}} = k_{\mathrm{B}}T\sum_j\nu_j N_{\mathrm{w}} \times\sum_i\left(\frac{\Theta_{ij}\left(1-\sum_k\Theta_{kj}\right)}{1-\sum_k\Theta_{kj}}\left(\frac{\partial\ln q_{ij}}{\partial V^{\mathrm{H}}}\right)_{T,N_{\mathrm{w}},\underline{\lambda}}\right) \quad \text{(A.44)}$$

where terms $(1-\sum_k\Theta_{kj})$ in the numerator and denominator cancel out resulting in

$$\Delta P^{\mathrm{H-EL}} = k_{\mathrm{B}}T\sum_j\nu_j N_{\mathrm{w}} \times\sum_i\left[\Theta_{ij}\left(\frac{\partial\ln q_{ij}}{\partial V^{\mathrm{H}}}\right)_{T,N_{\mathrm{w}},\underline{\lambda}}\right] \quad \text{(A.45)}$$

Recalling variations in $\ln q_{ij}$ from Eq. A.4 and variations in C_{ij} from Eq. A.10.

$$\Delta P^{\mathrm{H-EL}} = k_{\mathrm{B}}T \times\sum_j\left[\nu_j\sum_i\left[\Theta_{ij}\left(\frac{\partial\ln C_{ij}}{\partial\overline{V}^{\mathrm{EL}}}\right)_T\right]\right] \quad \text{(A.46)}$$

This is the final form of the pressure shift expression on a molecular basis.

The derivatives of Langmuir coefficients with respect to lattice molar volume are taken from numerical calculations according to Eq. A.39

Appendix A.5. The chemical potential of the host component

As before, to go from Eq. 37 to Eq. 38, we need to apply the expressions for derivatives of occupancy A.3.

$$\Delta\mu_{\mathrm{w}}^{\mathrm{H-EL}} = k_{\mathrm{B}}T \times\left(\frac{\partial\left(\sum_j\left[\nu_j N_{\mathrm{w}}\ln\left(1-\sum_i\Theta_{ij}\right)\right]\right)}{\partial N_{\mathrm{w}}}\right)_{V^{\mathrm{H}},T,\underline{\lambda}} \quad \text{(A.47)}$$

Also taking the chain rule on the differentiation of the logarithm function

$$\Delta\mu_{\mathrm{w}}^{\mathrm{H-EL}} = k_{\mathrm{B}}T\sum_j\left[\nu_j\ln\left(1-\sum_i\Theta_{ij}\right)\right] - k_{\mathrm{B}}T\sum_j\left[\frac{\nu_j N_{\mathrm{w}}}{1-\sum_i\Theta_{ij}} \times\left(\sum_i\left[\left(\frac{\partial\Theta_{ij}}{\partial N_{\mathrm{w}}}\right)_{T,V^{\mathrm{H}},\underline{\lambda}}\right]\right)\right] \quad \text{(A.48)}$$

where the derivatives of occupancy with respect to the number of water molecules are taken from Eq. A.2, variations in $\ln q_{ij}$ are taken from Eq. A.4 and variations in C_{ij} are taken from Eq. A.11.

$$\mu_{\mathrm{w}}^{\mathrm{H}} = \mu_{\mathrm{w}}^{EL} + k_{\mathrm{B}}T\sum_j\left[\nu_j\ln\left(1-\sum_i\left[\Theta_{ij}\right]\right)\right] + \overline{V}^{\mathrm{EL}}k_{\mathrm{B}}T\sum_j\nu_j\left(\sum_i\left[\Theta_{ij}\left(\frac{\partial\ln C_{ij}}{\partial\overline{V}^{\mathrm{EL}}}\right)_{T,N_{\mathrm{w}},\underline{\lambda}}\right]\right) \quad \text{(A.49)}$$

where Eq. A.46 contains a similar term which can be substituted here resulting in

$$\Delta\mu_{\mathrm{w}}^{\mathrm{H-EL}} = k_{\mathrm{B}}T\sum_j\left[\nu_j\ln\left(1-\sum_i\Theta_{ij}\right)\right] + \overline{V}^{\mathrm{EL}}\Delta P^{H-EL} \quad \text{(A.50)}$$

This is the final form of the relative chemical potential of water in the pressure shift model on a molecular basis.